学位論文

First-principles Study on Hydrogen Adsorption on Platinum Surfaces

(白金表面への水素吸着の第一原理計算)

平成 **26** 年 **7** 月 博士 **(**理学**)** 申請

東京大学大学院理学系研究科
物理学専攻

トラン ティ テュ ハン

Thesis

First-principles Study on Hydrogen Adsorption on Platinum Surfaces

TRAN THI THU HANH

The Department of Physics
The Graduate School of Science
The University of Tokyo

July 2014

Abstract

In recent years, much attention has been paid on hydrogen (H) atoms and molecules on a solid surface interfaced with liquid, especially H at the platinum (Pt) - solution interface. Many properties, including adsorption, diffusion, and vibration have been intensively studied. In spite of such efforts, however, theoretical understanding is still insufficient and there is much room for theoretical advancement. In this thesis the focus is put on removing known theoretical inconsistency regarding H on the Pt(111) surfaces and, through detailed comparison with experiment, justify the thermodynamic approach based on the density functional theory (DFT). The approach is then used to explore H on the Pt(110) surfaces. The present theoretical work is motivated by the aforementioned inconsistency regarding the most stable H site on the Pt(111) surfaces. Some calculations predicted the fcc site as the most stable one while others predicted the top site. Experimentally the fcc site was conjectured most stable from the electrochemical measurements while spectroscopic signal from the top site can be detected. Detailed comparison between theory and experiment is a key to settle this problem but most theory used very small lateral cell and provided only zero temperature properties, which cannot be directly compared with the measured thermodynamic data. Karlberg et al. [1] performed a Monte Carlo simulation using a parameter determined from DFT calculations but only the fcc site was assumed to exist. Our DFT calculation for H/Pt(111) reveals that the H adsorption energy depends very sensitively on the parameters adopted for the calculation and, to obtain reliable energy, large number of k-points and many Pt layers are required, which are much larger than those adopted by many foregoing researches. Then performing converged DFT calculations, the results were used to construct a lattice gas model with which we perform Monte Carlo simulations. The obtained isothermal adsorption properties were used to calculate the g-value, which reflects

the H-H interaction, as a function of the H coverage. The obtained g-value is in good agreement with the precise measurement, with the effective H-H interaction being underestimated only by 10 %. It is emphasized that the theory is most stringently tested by this comparison. From the comparison dominance of the fcc site is confirmed. The good agreement with experiment possibly suggests minor contribution of the hydration effect neglected in the present model. This theoretical approach is then applied to H on the missing row Pt(110)-(1×2). The dominant site is found to be the bridge site on the ridge, which is in agreement with the LEED experimental and DFT theoretical results found in the literature. The calculated g-value is in reasonable agreement in the lower coverage $\Theta_{\mathrm{H}} < 1/3$ conditions and in fair agreement for $\Theta_{\mathrm{H}} > 1/2$, while the theory predicts a distinct peak at $\Theta_{\mathrm{H}} \simeq 1/3$ although no such peak appears experimentally. The inconsistency with experiment will indicate that the present modeling with the missing row structure only is questionable and further calculation is then necessary to explain the experiment.

Contents

Chapter 1

Introduction

Materials exhibit wide variety of functionality originating from infinite combinations of arranging large number of atoms and molecules. Elucidation of the material functionality includes search for the relationship between the microscopic world and the macroscopic one, which has long been a challenging theme of physics and materials science. Today the research has become more and more quantitative. The material functionality does not only reflect its bulk properties but also, or often more importantly, reflects its surface/interface properties, which fact has motivated researches on the surfaces and interfaces. This is particularly the case for the study of catalytic functionality, where even a slight change in the surface structure and/or surface stoichiometry can completely change the functionality. Among others, platinum surfaces as well as noble metal surfaces offer the most ideal model systems for such research because both the catalytic functionality and the surface/interface structures can be most precisely controlled and measured. Indeed, owing to recent advances in the technology, it is possible to provide atomically flat interface of a solid and a liquid as well as atomically flat interface of a solid and the ultrahigh vacuum (UHV). It is noteworthy that a scanning tunneling microscopy (STM) has confirmed such flat interface is indeed realized between a metal surface and the solution [2]. The realized system, called as model catalyst, has opened a way to relate the surface structure and the catalytic functionality.

Despite the advances in preparing the interface (or the buried surface), microscopic characterization of the interface has been hampered by the intense signal from the bulk. To extract signal from the interface, novel surface sensitive experimental methods have been developed such as infrared resection-absorption spectroscopy (IRAS) [3], the sum frequency generation (SFG) [4], the Fourier transform infrared adsorption spectra (FT-IRAS) [5], and the Raman spectroscopy (RS) [6]. Such apparatuses have been combined with the traditional electrochemical methods such as cyclic voltammetry (CV) [7, 8, 9, 10, 11] to significantly advance understanding of the interface structures and atoms/molecules adsorbed at the interfaces. Yet, it is still extremely difficult to capture atomic processes leading to catalysis because the process is often too fast to detect experimentally. In this context, the first-principles calculation has attracted considerable attention.

As a tool to investigate the surfaces in UHV, the first-principles calculation has shown great success. In the case of the surfaces in UHV, one can use the surface structures determined experimentally or those optimized within the theory to

investigate the properties of the surface. In the case of the solid/liquid interface, however, things are different. The liquid structures fluctuate rapidly and the theory needs to deal with the statistics of the liquid structures. This is a heavy burden of the calculation and it is still infeasible to take it fully into account. Instead, the UHV surface approach has been applied to the problem of *hydrophobic* interfaces where interaction with the solution is weak. The approach has been considered valid for platinum or other noble metal and large number of calculations can be found in the literatures [12, 13]. Although the approach generally provides consistent explanation of experiments, detailed comparison with precise measurement (or accurate calculation of the interface) has been lacking. It is very important to show how the UHV approach is accurate or inaccurate in describing the buried surface.

One of the aims of the present thesis is to elucidate the hydrogen electroadsorption from the first-principles calculation, the Monte Carlo simulation, and the electrochemical data. We are trying to provide an example where theory and experiment are seriously compared to examine if the g-value can be accurately predicted. We also want to advance understanding of the electroadsorption.

The target of the present study is the effective interaction of adsorbed hydrogen atoms on platinum surfaces. The interaction depends strongly on the surface structures. According to the CV experiment [11, 14], the interaction is repulsive on Pt(111) and the repulsion is much weaker on Pt(100) and Pt(110). When interfaced with H_2SO_4 solution, the interaction is attractive on Pt(100) and Pt(110). These results were obtained from the CV measurement by determining the Gibbs free-energy of H-adsorption (ΔG), and then to obtain the H coverage derivative of ΔG, which corresponds to the energy cost of adsorbing additional H atom. The latter quantity corresponds to the effective H-H interaction, and plays a very important role in determining the surface coverage and the catalytic activity of the surface. What is important in the present study is that the adsorption isotherm is systematically determined for various surfaces with the zero point energy (ZPE) correction of quantum effect, which has never been calculated in foregoing theoretical studies. Therefore, by comparing these data with theory, it is possible to diagnose the accuracy of theory. When ΔG is calculated accurately using a model that neglects the hydration effect, the comparison provides information on the strength of the hydration. Among others, Pt(111) is the simplest surface where calculation can be done most accurately. In this context, the problem of H/Pt(111) is used for testing the UHV surface model.

In doing the theoretical calculation of H/Pt(111), it is worth mentioning that many forgoing calculation [15, 16, 17, 18, 19, 20, 21, 22, 23, 24, 25] did not lead to the same conclusion regarding the most stable adsorption site. Some studies showed that the top site is the most stable site [15, 18, 21], while others found that the fcc is more stable than the top [22, 25]. This happened despite the fact that those calculations commonly used the density functional theory (DFT) within the generalized gradient approximation (GGA) for the exchange-correlation energy. This is due to insufficient parameters for the DFT-GGA calculation, in particular, insufficient number of k-points in the Brillouine zone integration and insufficient number of Pt layers for the slab model. In this context the present research started from accurate

determination of the H adsorption energy within DFT-GGA. The calculated adsorption energy is then used to compute the effective H-H interaction. We will focus on the comparison of the effective H-H interaction, or the g-value, using a Monte Carlo simulation on a lattice gas model parameterized. Note that a similar Monte Carlo simulation was done by Karlberg *et al.* [23] using the fcc site only to compare the theoretical and experimental isotherm, $\Theta_{\mathrm{H}}(U)$, but here we use both the fcc and the top sites and compare the derivative of the isotherm, which corresponds to the g-value. We examine if the lattice gas model successfully accounts for the experiment or it needs adjustment of the parameters. Discrepancy from the experiment should be ascribed to the hydration effect and/or the DFT-GGA error albeit it is not possible to discuss relative importance. The comparison nevertheless provides important insight into the H-adsorption, which prompts further theoretical investigation. For the H/Pt(110), the modeling is more complex. For the face-centered cubic FCC(110) surfaces, the unreconstructed (1×1) phase and the reconstructed (1×2) phase with missing-row exist. The (1×1) unit cell contains one substrate atom on the outermost row, the second and third layer atoms are still fairly exposed [26]. The (1×2) unit cell contains four more or less exposed Pt atoms [27, 28]. In practical applications, the Pt catalyst is often finely dispersed in small particles embedded in a matrix and the active sites can be of various types, such as, edges where crystal facets meet. The missing row reconstructed Pt(110)-(1×2) surface is a convenient model for the edge sites formed between the most stable facets, or Pt(111). This fact motivated almost all theoretical calculations to use the missing row Pt(110)-(1×2) [27, 28, 29, 30, 31], reproducing thereby reasonable properties of the most stable adsorption site. The modeling, however, has not been seriously tested. It is worth investigating if the effective H-H interaction can be reproduced by the missing row Pt(110)-(1×2) model. So, this thesis focuses on comparing in detail the effective H-H interaction to diagnose the model.

In this thesis, chapter 2 is devoted to the summarization of foregoing studies of hydrogen electroadsorption on the Pt surface. Chapter 3 is devoted to the methods adopted in the present research. In chapter 4, the first-principles thermodynamic study on Pt(111) surface is presented. The research on the missing row Pt(110)-(1×2) surface is given in chapter 5. In chapter 6, summary and conclusion are described.

Chapter 2

Background

2.1 Hydrogen electroadsorption

The phenomenon of the hydrogen electroadsorption, i.e., adsorption at the electrode solution interface, is quite distinct from the hydrogen adsorption on the UHV surface. The peculiar aspect is explained in this section.

Hydrogen electroadsorption can be accomplished from either acidic or basic aqueous solutions as well as from non-aqueous solutions that are capable of dissolving H-containing acids. The hydrogen can be alternatively supplied from solvents that are automatically dissociated to form proton. The proton, H^+, cannot exist by itself in aqueous acidic solution and it combines readily with a non-bonding electron pair of a water molecule forming H_3O^+ [8, 32, 33, 34, 35]. In the vicinity of the electrode, H_3O^+ discharges to form the electroadsorbed H [8, 32, 33, 35, 36, 37, 38] according to the following single-electrode process:

$$M + H^+ + e^- \xrightarrow{E} M\text{-}H_{ads}, \tag{2.1}$$

where M stands for a surface atom of the metal substrate and E represents the electrode potential. Importantly, this process can be precisely controlled by changing the electrode potential. The electroadsorbed hydrogen can undergo the subsequent reactions [33, 34]:

$$H^+ + e^- + M\text{-}H_{ads} \xrightarrow{E} M + H_2 \tag{2.2}$$

or

$$2M\text{-}H_{ads} \rightarrow 2M + H_2. \tag{2.3}$$

Equations (2.2) and (2.3), which follow the step (2.1), are the alternative pathways of the hydrogen evolution reaction (HER), namely (2.1)-(2.2) represent the Volmer-Heyrovsky pathway, whereas (2.1)-(2.3) stand for the Volmer-Tafel step.

By changing the electrode potential, the chemical equilibrium can be shifted such that at the potential more negative (positive) than the equilibrium potential, the reactions (2.1)-(2.3) proceed forward (backward). The standard electrode potential is defined as the reversible potential at the standard condition, i.e., at room temperature, 1 atm for the pressure, and 1 for the pH. Unless such conditions are

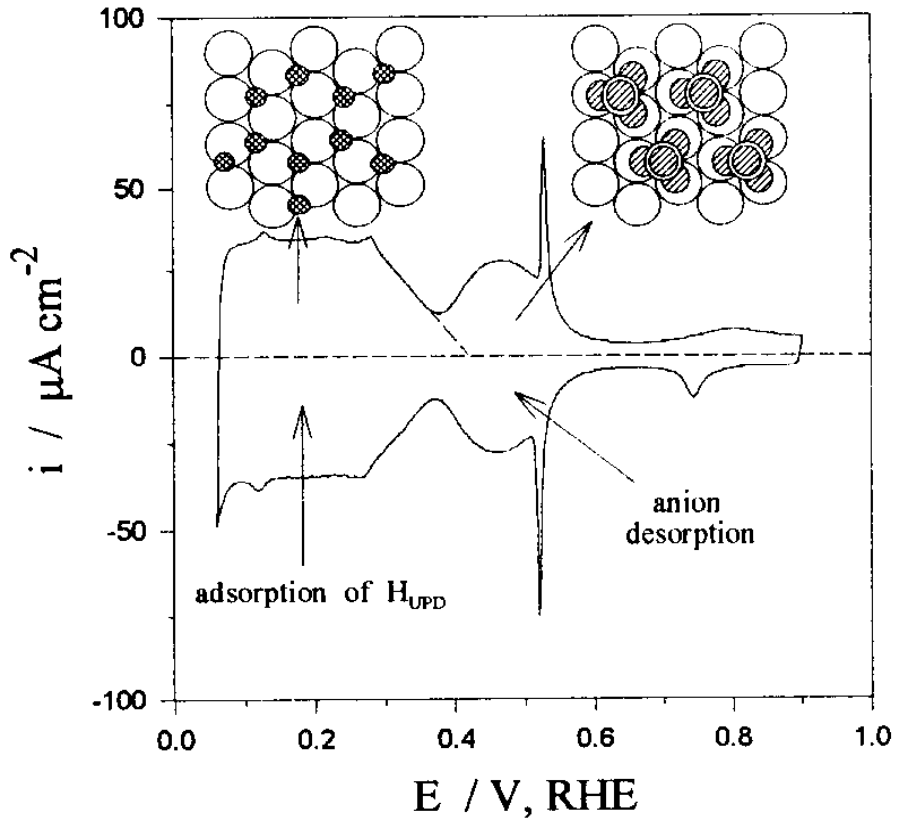

Figure 2.1: Cyclic-voltammetry profile for Pt(111) in 0.05 M aqueous H_2SO_4 showing the regions of the UPD H and anion adsorption with schematic representation of their structures; scan rate, $s = 50mVs^{-1}$ and T=298 K [36, 37, 38, 39].

delicately concerned, the standard electrode potential (SHE) and the reversible hydrogen electrode potential (RHE) will not be carefully distinguished in this thesis.

Historically the electroadsorbed hydrogen is distinguished according to the condition at which it is adsorbed: (i) the under-potential deposition of H (H_{upd}), and (ii) the over-potential deposition of H (H_{opd}). The H_{upd} takes place above the thermodynamic reversible potential of the HER (E^0_{HER}), and the process is known to occur at Pt, Rh, Pd and Ir electrodes (Fig. 2.1). On the other hand, the overpotential deposition of H (H_{opd}) takes place at potentials below E^0_{HER} on all metallic and conducting-composite surfaces at which the HER can occur [8]. Thus, the H_{upd} in aqueous solutions is a phenomenon characteristic of only certain noble metals. This thesis focuses only on the electroadsorption under the underpotential region. Note that neither H_{upd} nor H_{opd} is distinguished according to the adsorption site although the fcc hollow site and the top site are considered the major site for H_{upd} and H_{opd}, respectively as indicated in Figure 2.1.

2.2 Electrochemical Adsorption Isotherms

In studying the electroadsorption, the most relevant quantities are the thermodynamic state functions for the adsorption, such as Gibbs energy (ΔG^0_{ads}), enthalpy

($\Delta H^0_{\rm ads}$), and entropy ($\Delta S^0_{\rm ads}$), where the superscript (^{0}) means to take the value referring to that at the standard condition. Generally, those quantities sensitively depend on the hydrogen coverage because of the lateral interaction between the adsorbed hydrogen atoms. It is therefore important to carefully determine the interaction and the coverage consistently. The enthalpy $\Delta H^0_{\rm ads}$ assesses the nature of the strength of the hydrogen-surface bonding $E_{\rm M\text{-}H_{ads}}$ [7, 8, 9, 11, 36]. The values for $\Delta G^0_{\rm ads}$, $\Delta H^0_{\rm ads}$, $\Delta S^0_{\rm ads}$, and $E_{\rm M\text{-}H_{ads}}$ have been determined experimentally by analyzing the measured data using model adsorption isotherms.

2.2.1 Basic equations

$\rm H_{upd}$ is adsorbed at the interface when the potential is more positive than the reversible potential through Eq. (2.1), which will be rewritten now as

$$\rm M + H^+ + \mathit{e}^- \rightarrow M\text{-}H_{ads}, \tag{2.4}$$

where M is the metal site on the electrode surface, $\rm H^+$ is the hydrated proton (which is more often written as $\rm H_3O^+$), $\rm e^-$ is the electron at the electrode, and $\rm H_{ads}$ is the hydrogen atom adsorbed on the electrode. The potential at the electrode is referred to as the vacuum level near the solution and is assigned as $\phi^{\rm M}$, so that the energy of the electron in the electrode, E_F (Fermi level of the electrode), is given as

$$E_F = -e\phi^{\rm M}, \tag{2.5}$$

where the negative sign comes from the negative charge of the electron. The equilibrium condition for the reaction (2.4) is

$$\mu_{\rm M} + \bar{\mu}_{\rm H^+} + \bar{\mu}^M_{e^-} = \mu_{\rm M\text{-}H}, \tag{2.6}$$

where $\mu_{\rm M}$ is the chemical potential (i.e., the Gibbs free-energy per particle) of the electrode (M), $\bar{\mu}_{\rm H^+}$ is the electrochemical potential ($\bar{\mu}$) of the hydrated proton, $\bar{\mu}^{\rm M}_{e^-}$ is the electrochemical potential of the electron in the electrode (M), and $\mu_{\rm M\text{-}H}$ is the chemical potential of the electrode adsorbed with the hydrogen atoms. Using Eq. (2.5), Eq. (2.6) becomes

$$-e\phi^{\rm M} = \bar{\mu}^{\rm M}_{e^-} = \mu_{\rm M\text{-}H} - \mu_{\rm M} - \bar{\mu}_{\rm H^+}. \tag{2.7}$$

When the electrode potential $\phi^{\rm M}$ is equal to a special value, say $\phi^{\rm M'}$, the reaction

$$\rm H^+ + \mathit{e}^- \rightarrow \frac{1}{2}H_2 \tag{2.8}$$

will be in equilibrium under the standard condition. The value of $\phi^{\rm M'}$ is called the standard electrode potential and is often used as the reference potential. Then, the following relations hold:

$$\bar{\mu}^0_{\rm H^+} + \bar{\mu}^{\rm M'}_{e^-} = \frac{1}{2}\mu^0_{\rm H_2} \tag{2.9}$$

or

$$\bar{\mu}^0_{\mathrm{H}^+} - e\phi^{\mathrm{M}'} = \frac{1}{2}\mu^0_{\mathrm{H}_2}. \tag{2.10}$$

Using Eqs. (2.7) and (2.10), the following important equation is obtained:

$$-e(\phi^{\mathrm{M}} - \phi^{\mathrm{M}'}) \equiv -e\eta = \mu_{\text{M-H}} - \mu_{\mathrm{M}} - \frac{1}{2}\mu^0_{\mathrm{H}_2} - (\bar{\mu}_{\mathrm{H}^+} - \bar{\mu}^0_{\mathrm{H}^+}), \tag{2.11}$$

where η measures the deviation from the standard potential and is called overpotential. Eq. (2.11) is the starting point of the electrochemical analysis.

2.2.2 Adsorption isotherm

Consider the condition at which the reaction (2.4) is in equilibrium. The condition will be given by the number of the hydrogen atoms adsorbed on the surface

$$N_{\text{M-H}} \equiv N_{\text{sites}}\Theta_{\mathrm{H}},$$

the number of sites on which additional hydrogen can be adsorbed

$$N_{\text{sites}}(1-\Theta_{\mathrm{H}}),$$

and the number of the hydrated proton N_{H^+} near the electrode surface. Assuming the Boltzmann distribution, N_{H^+} will be given as

$$N_{H^+} \propto \exp[-\beta\bar{\mu}_{\mathrm{H}^+}].$$

The microscopic equilibrium condition says that the ratio of the product over the reactant is determined only by the reaction constant α such that:

$$\frac{N_{\text{sites}}\Theta_{\mathrm{H}}}{N_{\text{sites}}(1-\Theta_{\mathrm{H}})} = \alpha. \tag{2.12}$$

From Eq. (2.11) we find that

$$N_{H^+} \propto \exp\left[-\beta\left(\mu_{\text{M-H}} - \mu_{\mathrm{M}} - \frac{1}{2}\mu^0_{\mathrm{H}_2} + e\eta\right)\right], \tag{2.13}$$

and from Eqs. (2.12) and (2.13) we obtain

$$-k_BT\ln\frac{\Theta_{\mathrm{H}}}{1-\Theta_{\mathrm{H}}} = \mu_{\text{M-H}} - \mu_{\mathrm{M}} - \frac{1}{2}\mu^0_{\mathrm{H}_2} + e\eta + \text{const} \tag{2.14}$$

or

$$-e\eta - k_BT\ln\frac{\Theta_H}{1-\Theta_H} = \mu_{\text{M-H}} - \mu_{\mathrm{M}} - \frac{1}{2}\mu^0_{\mathrm{H}_2} + \text{const} = G^0_{\text{ads}}(\mathrm{H}) + \text{const}. \tag{2.15}$$

Here $G^0_{\text{ads}}(\mathrm{H})$ is the Gibbs free-energy for adsorption

$$G^0_{\text{ads}}(\mathrm{H}) = \mu_{\text{M-H}} - \mu_{\mathrm{M}} - \frac{1}{2}\mu^0_{\mathrm{H}_2}.$$

When taking derivative with respect to Θ_{H}, we get

$$\frac{dG^0_{\mathrm{ads}}(\mathrm{H})}{d\Theta_{\mathrm{H}}} = -e\frac{d\eta}{d\Theta_{\mathrm{H}}} - k_BT\frac{\ln\frac{\Theta_{\mathrm{H}}}{1-\Theta_{\mathrm{H}}}}{d\Theta_{\mathrm{H}}} = -e\frac{d\eta}{d\Theta_{\mathrm{H}}} - k_BT\left(\frac{1}{\Theta_{\mathrm{H}}} + \frac{1}{1-\Theta_{\mathrm{H}}}\right). \tag{2.16}$$

By integrating with respect to Θ_{H}, we get

$$-e[\eta(\Theta_{\mathrm{H}}) - \eta(\Theta^0_{\mathrm{H}})] = G^0_{\mathrm{ads}}(H,\Theta_H) + k_BT\ln\frac{\Theta_{\mathrm{H}}}{1-\Theta_{\mathrm{H}}} - \left\{G^0_{\mathrm{ads}}(\mathrm{H},\Theta^0_{\mathrm{H}}) + k_BT\ln\frac{\Theta^0_{\mathrm{H}}}{1-\Theta^0_{\mathrm{H}}}\right\}, \tag{2.17}$$

where $\eta(\Theta^0_{\mathrm{H}})$ is zero.

Below this equation is investigated for special cases where the adsorbed H atoms do not interact (Langmuir isotherm) and the interaction is described by a simple formula (Frumkin isotherm).

2.2.3 Langmuir isotherm

The electrochemical Langmuir isotherm describes the adsorption of adsorbate onto the surface following three assumptions [40, 41, 42]: (i) the Gibbs energy of adsorption is potential dependent; (ii) the coverage is potential dependent in the sense that a complete monolayer can be formed upon potential variation; and (iii) there are no lateral interactions between the species adsorbed on the electrode surface. The Gibbs energy of adsorption does not vary with the H surface coverage (Θ_{H}), that is

$$G^0_{\mathrm{ads}}(H)_{\Theta_{\mathrm{H}}=0} = G^0_{\mathrm{ads}}(H)_{\Theta_{\mathrm{H}}\neq 0}, \tag{2.18}$$

and we obtain

$$\frac{\Theta_{\mathrm{H}}}{1-\Theta_{\mathrm{H}}} = a_{\mathrm{H}^+}\exp\left(-\frac{e\eta}{k_BT}\right)\exp\left(-\frac{G^0_{\mathrm{ads}}(\mathrm{H})}{k_BT}\right), \tag{2.19}$$

where a_{H^+} is the activity of H^+ in the electrolyte bulk.

In the case of Langmuir isotherm, the chemical potential of the electrode adsorbed with the hydrogen atoms ($\mu_{\mathrm{M\text{-}H}}$) is expressed as [14, 43]

$$\mu_{\mathrm{M\text{-}H}} = \mu^0_{\mathrm{M\text{-}H}}(\Theta_{\mathrm{H},r} = 0.5) + k_BT\ln\left(\frac{\Theta_{\mathrm{H}}}{1-\Theta_{\mathrm{H}}}\right), \tag{2.20}$$

where it has been assumed only in this subsection that the coverage is 0.5 at the standard electrochemical potential following a historical convention [35]. In such a case, using Eq. (2.20) into Eq. (2.11), the adsorption isotherm will be

$$\begin{aligned} -\frac{e\eta}{k_BT} - \ln\frac{\Theta_{\mathrm{H}}}{1-\Theta_{\mathrm{H}}} + \bar{\mu}_{\mathrm{H}^+} - \bar{\mu}^0_{\mathrm{H}^+} &= \frac{\mu^0_{\mathrm{M\text{-}H}}(\Theta_{\mathrm{H},r}=0.5) - \mu^0_{\mathrm{M}} - \frac{1}{2}\mu^0_{\mathrm{H}_2}}{k_BT} \\ &= \frac{G^0_{\mathrm{ads}}(\Theta_{\mathrm{H},r}=0.5)}{k_BT}. \end{aligned} \tag{2.21}$$

This equation was developed in [35] using the Born-Haber cycle but the use of electrochemical potentials makes it simpler and more straightforward.

In reality, the adsorption isotherm is more complex because of the interaction of H atoms [14] and Eq. (2.20) should be corrected like

$$\mu_{\text{M-H}} = \mu^0_{\text{M-H}}(\Theta_{\text{H},r} = 0.5) + r(\Theta_{\text{H}}) + k_B T \ln\left(\frac{\Theta_{\text{H}}}{1-\Theta_{\text{H}}}\right) \tag{2.22}$$

with the correction term $r(\Theta_{\text{H}})$ corresponding to the effective H-H interaction energy, and Eq. (2.21) as

$$\begin{aligned} -\frac{e\eta}{k_B T} - \ln\left(\frac{\Theta_{\text{H}}}{1-\Theta_{\text{H}}}\right) + \bar{\mu}_{\text{H}^+} - \bar{\mu}^0_{\text{H}^+} &= \frac{G^0_{\text{ads}}(\Theta_{\text{H},r} = 0.5)}{k_B T} + \frac{r(\Theta_{\text{H}})}{k_B T} \\ &= U^0 + h(\Theta_{\text{H}}) \\ &\equiv \frac{G^a_{\text{ads}}}{k_B T}, \end{aligned} \tag{2.23}$$

where $h(\Theta_{\text{H}}) = r(\Theta_{\text{H}})/k_B T$ is the dimensionless interaction energy, U^0 is the dimensionless standard adsorption energy and $G^{\text{a}}_{\text{ads}}$ is the corrected adsorption energy that depends on the hydrogen surface coverage through the interaction term $r(\Theta_{\text{H}})$ [14]. The reference state surface coverage $\Theta_{\text{H,r}}$ has been historically defined as the one where the second and the third terms in Eq. (2.22) cancels and thus the following equation holds [43, 44, 45]

$$\mu_{\text{M-H}}(\Theta_{\text{H}}) = \mu^0_{\text{M-H}}(\Theta_{\text{H},r} = 0.5).$$

Then Eq. (2.23) is [14]

$$h(\Theta_{\text{H}}) + \ln\frac{\Theta_{\text{H}}}{1-\Theta_{\text{H},r}} = -\frac{e\eta_r}{k_B T} + \frac{G^0_{\text{ads}}(\Theta_{\text{H},r} = 0.5)}{k_B T} = 0. \tag{2.24}$$

2.2.4 Frumkin isotherm

The Frumkin adsorption isotherm takes into account the long-range interactions between the adsorbed species [40, 42, 46, 47], i.e.

$$\frac{\Theta_{\text{H}}}{1-\Theta_{\text{H}}} = a_{\text{H}^+} \exp\left(-\frac{e\eta}{k_B T}\right) \exp\left(-\frac{G^0_{\text{ads}}(\text{H})_{\Theta_{\text{H}}=0}}{k_B T}\right) \exp\left(-g\Theta_{\text{H}}\right), \tag{2.25}$$

where g is the dimensionless interaction parameter and it has negative values for attractive interactions and positive ones for repulsive interactions [8]. The Frumkin isotherm assumes linear relation between the Gibbs energy of adsorption and Θ_{H} according to the formula:

$$G^0_{\text{ads}}(\text{H})_{\Theta_{\text{H}}\neq 0} = G^0_{\text{ads}}(\text{H})_{\Theta_{\text{H}}=0} + g k_B T \Theta_{\text{H}}. \tag{2.26}$$

As expected on the ground of the above relation, $G^0_{\text{ads}}(\text{H})$ increases towards less negative values in presence of repulsive interactions between the adsorbed species

and towards more negative ones in presence of attractive interactions [8].

In the case of the Frumkin isotherm, the dimensionless interaction energy is a linear function of Θ_{H}

$$h(\Theta_H) = g\Theta_H. \tag{2.27}$$

In general, the interaction parameter h may also depend on the adsorption of ions or other species on the electrode surface: $h(\Theta_{\mathrm{H}}, \Theta_i)$ where Θ_i is the coverage of species i [14]. To determine $h(\Theta_{\mathrm{H}})$ it is necessary to integrate the experimentally accessible parameter $dh(\Theta_{\mathrm{H}})/d\eta$. It is also possible to determine the derivative $dh/d\Theta_{\mathrm{H}}$ more directly using Eq. (2.23) [14]

$$\frac{dh}{d\Theta_{\mathrm{H}}} = -\frac{e}{k_B T}\frac{d\eta}{d\Theta_{\mathrm{H}}} - \frac{1}{\Theta_{\mathrm{H}}(1-\Theta_{\mathrm{H}})}. \tag{2.28}$$

2.3 Determination of H_{upd} isotherms on Pt(hkl)

The cyclic-voltammetry (CV), also referred to as potential-stimulated adsorption-desorption (PSAD) [48], is a convenient technique. It can be applied to research on adsorption of ionic species, such as proton to be under-potential deposited on the surface, semiconductor and metallic species as well as specific adsorption of anions [8]. Juan Feliu and his group investigated the cyclic voltammograms of Pt(hkl) in 0.1 M perchloric and 0.5 M sulfuric and acid in 1993 (see Fig. 2.2) [49, 50, 51]. Later, this interesting research on thermodynamics of the H_{upd} on well-defined Pt(hkl) electrodes were continued intensively studying by Zolfaghari et al. (Fig. 2.3) [48, 52, 53], Marković et al. (Fig. 2.4) [7, 10, 11].

The experimental cyclic voltammograms from Feliu et al. [50] were corrected for the capacitive current assuming it is constant in the whole potential range. The current density is simply related to $d\Theta/dE$:

$$j = \sigma_1 \upsilon \frac{d\Theta_{\mathrm{H}}}{dE}, \tag{2.29}$$

where σ_1 is the charge necessary for a monolayer coverage and υ is the sweep rate [14]. The experimental curves were corrected for the additional contributions arising from other processes and the corrected curves were analyzed to obtain thermodynamic parameters of H adsorption.

Using Eq. (2.23) it is possible to determine the Gibbs energy of adsorption

$$\Delta G^a_{\mathrm{ads}}(\Theta_{\mathrm{H}}) = \Delta G^0_{\mathrm{ads}}(\Theta_{\mathrm{H},r}) + h(\Theta_{\mathrm{H}})$$

and, from Eq. (2.28), the derivative $dh/d\Theta_{\mathrm{H}}$ [14]. The derivatives $dh/d\Theta_{\mathrm{H}}$ for Pt(111), Pt(100) and Pt(110), obtained by Lasia, are shown in Fig. 2.5 [14]. They are determined directly from the experimental data $d\Theta_{\mathrm{H}}/d\eta$. Note that the results contain rich physics. Besides, for Pt(111), the value of $g = 12$ was found by Marković et al. in $HClO_4$ [10] and $g = 11$ was found by Zolfaghari and Jerkiewicz H_2SO_4 [9]. The thermodynamic parameters of hydrogen upd on Pt(hkl), obtained by Lasia [14], are shown in Table 2.1.

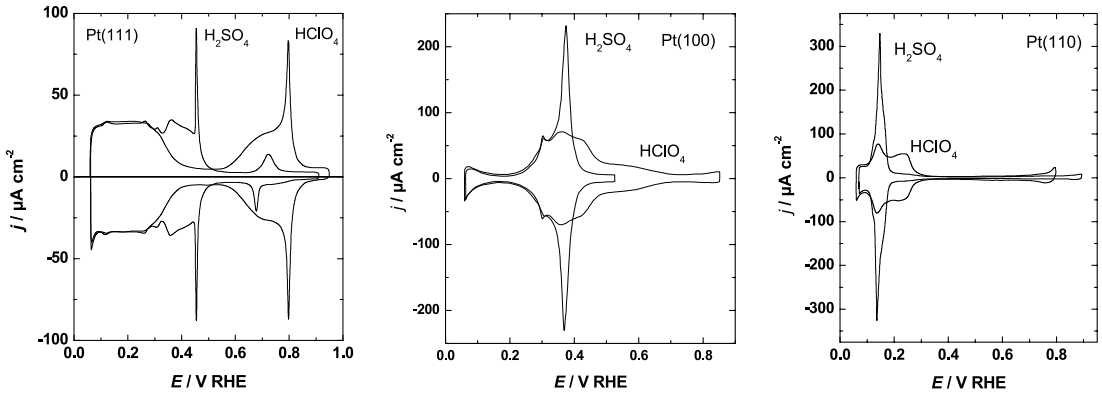

Figure 2.2: Cyclic voltammograms of Pt(111), Pt(100) and Pt(110) in 0.5 M H_2SO_4 and 0.1 M $HClO_4$ at a sweep rate of 50 mV s^{-1} [49, 50, 51].

It is interesting to notice that the dependence of the Gibbs energy of adsorption, $\Delta G^{\mathrm{a}}_{\mathrm{ads}}$, and the interaction parameter, $h(\Theta_{\mathrm{H}})$ on Θ_{H} in perchloric acid indicates repulsive interactions between adsorbed hydrogen atoms, with the interaction parameter ranging from 2.0 at Pt(100), 11.9 at Pt(111) to 2.9 (at low Θ_{H}) for Pt(110). Differences in behavior between Pt(100) and Pt(110) are surprising. It is possible that this behavior is connected with some surface reconstruction occurring on Pt(110) [14].

In H_2SO_4 on Pt(100), the interactions are attractive at low Θ_{H} and repulsive at high Θ_{H} (although the total adsorption energy does not change much) while on Pt(110) attractive interactions are observed in the whole range of Θ_{H}. Because of the similarity between the cyclic voltammetric curves on Pt(111) in both acids, similar repulsive interactions are concluded [14].

It should also be mentioned that in the case of Pt(100) in H_2SO_4 and Pt(110) in $HClO_4$ there is a change in the slope of $\Delta G^{\mathrm{a}}_{\mathrm{ads}}/k_B T$ with Θ_{H} indicating changes of the type of interactions: attractive at low and repulsive at high Θ_{H} although total changes of this parameter are smaller in other cases. Apparent attractive interactions are result of easy adsorption of hydrogen after desorption of bisulfate [14]. The experimental results indicate that a simple Frumkin type isotherm may well describe the hydrogen adsorption reaction for Pt(100) in $HClO_4$, Pt(110) in H_2SO_4 and Pt(111) in $HClO_4$ over the whole potential range.

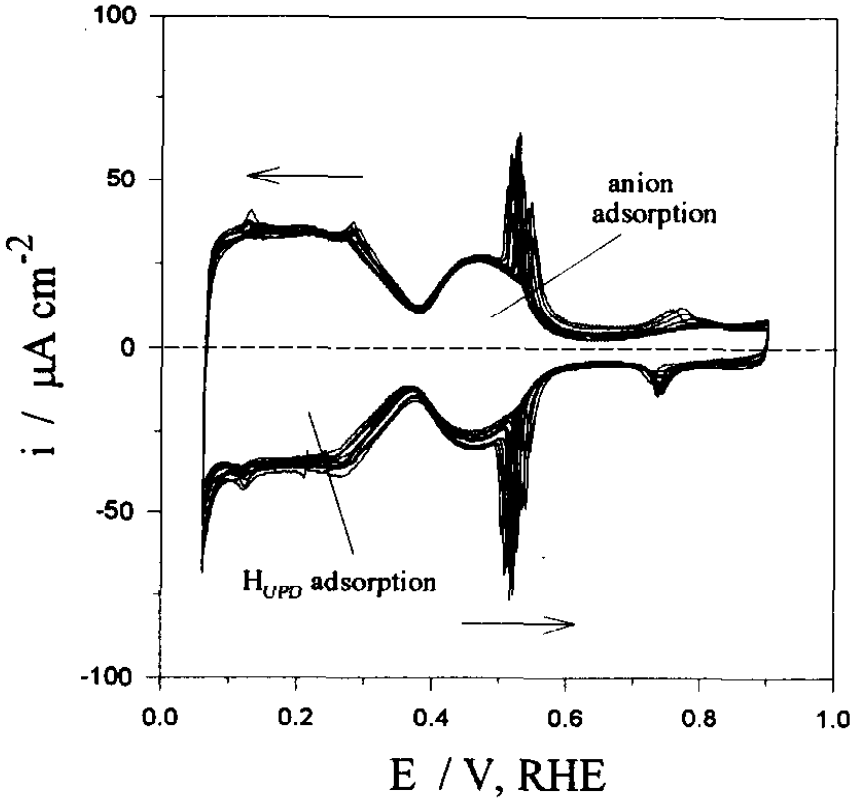

Figure 2.3: Series of CV profiles for Pt(111) in 0.05 M aqueous H_2SO_4 solution at $273K \leq T \leq 328K$ with $\Delta T = 5K$; s=50 mV s^{-1} and $A_r = 0.058cm^2$. Arrows indicate changes caused by T variation [48, 52, 53].

Electrode	Pt(100)	Pt(110)	Pt(111)
$HClO_4$			
$\Delta G^0_{ads}(\Theta_{H,r})/k_BT$	-15.16±0.005	-8.60±0.04	-10.49±0.05
$\Delta G^0_{ads}(\Theta_{H,r})/kJmol^{-1}$	-38	-21	-26
$\Theta_{H,r}$	0.31	0.35	0.145
$g = d(\Delta G^a_{ads}/k_BT)/d\Theta_H$	2.0±0.1	2.9±0.1 low Θ ~ 0 high Θ	11.9±0.1
$g = d(h)/d\Theta_H$	~ 2.5	Not constant	11.2-12.8
H_2SO_4			
$\Delta G^0_{ads}(\Theta_{H,r})/k_BT$	-12.9	-4.22±0.01	
$\Delta G^0_{ads}(\Theta_{H,r})/kJmol^{-1}$	-32	-10.5	
$\Theta_{H,r}$	0.74	0.984	
$g = d(\Delta G^a_{ads}/k_BT)/d\Theta_H$	-2.5 low Θ 2.45 high Θ	-3.04±0.02	
$g = d(h)/d\Theta_H$	-2 to -3	-3.1	

Table 2.1: Thermodynamic parameters of H upd on Pt(khl) [14]

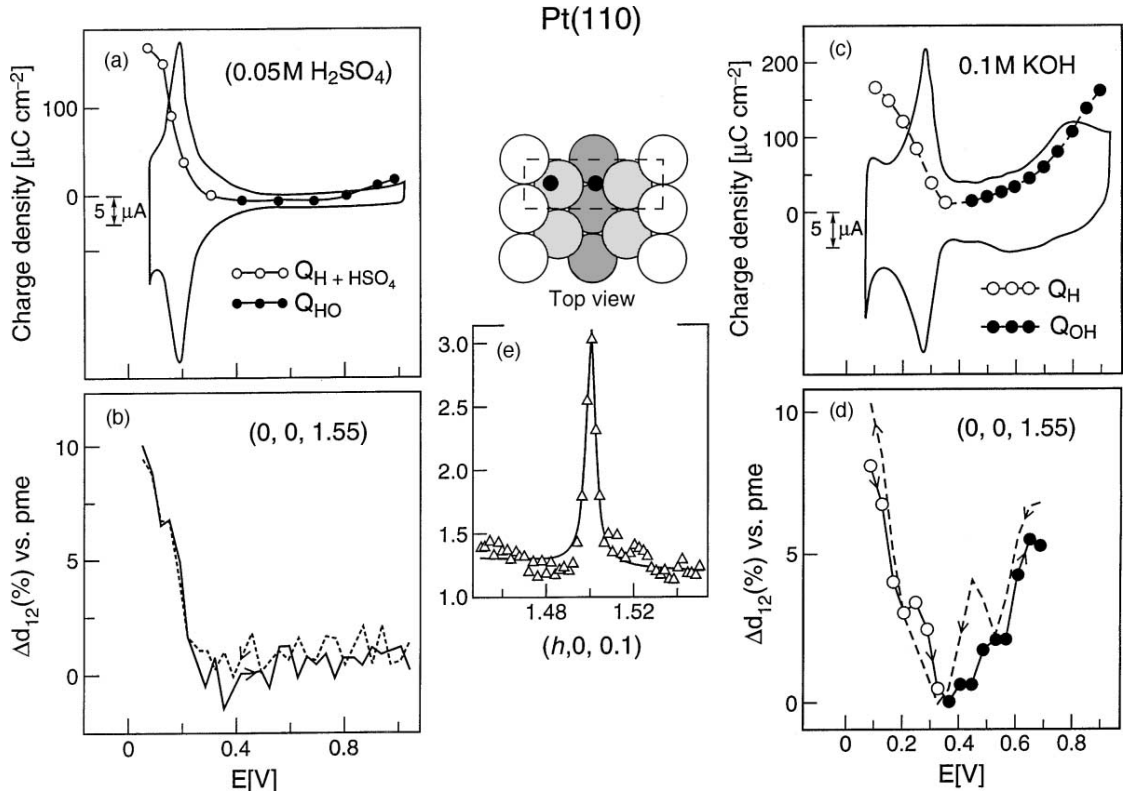

Figure 2.4: Cyclic voltammetry of the Pt(110)-(1×2) surface in electrochemical cell: (a) in H_2SO_4 and (c) in 0.1 M KOH. The potential was scanned at 50 mV/s. Changes in inter-layer spacing (Δd_{12}) measured on scanning the potential at 2 mV/s (b) in H_2SO_4 and (d) in 0.1 M KOH. (e) The measured X-ray intensity at (0, 1.5, 0.1) along the [0 1 0] direction along with an ideal model for the (1×2) structure: solid dots represent H_{upd} and OH_{rv}. E vs. RHE [10].

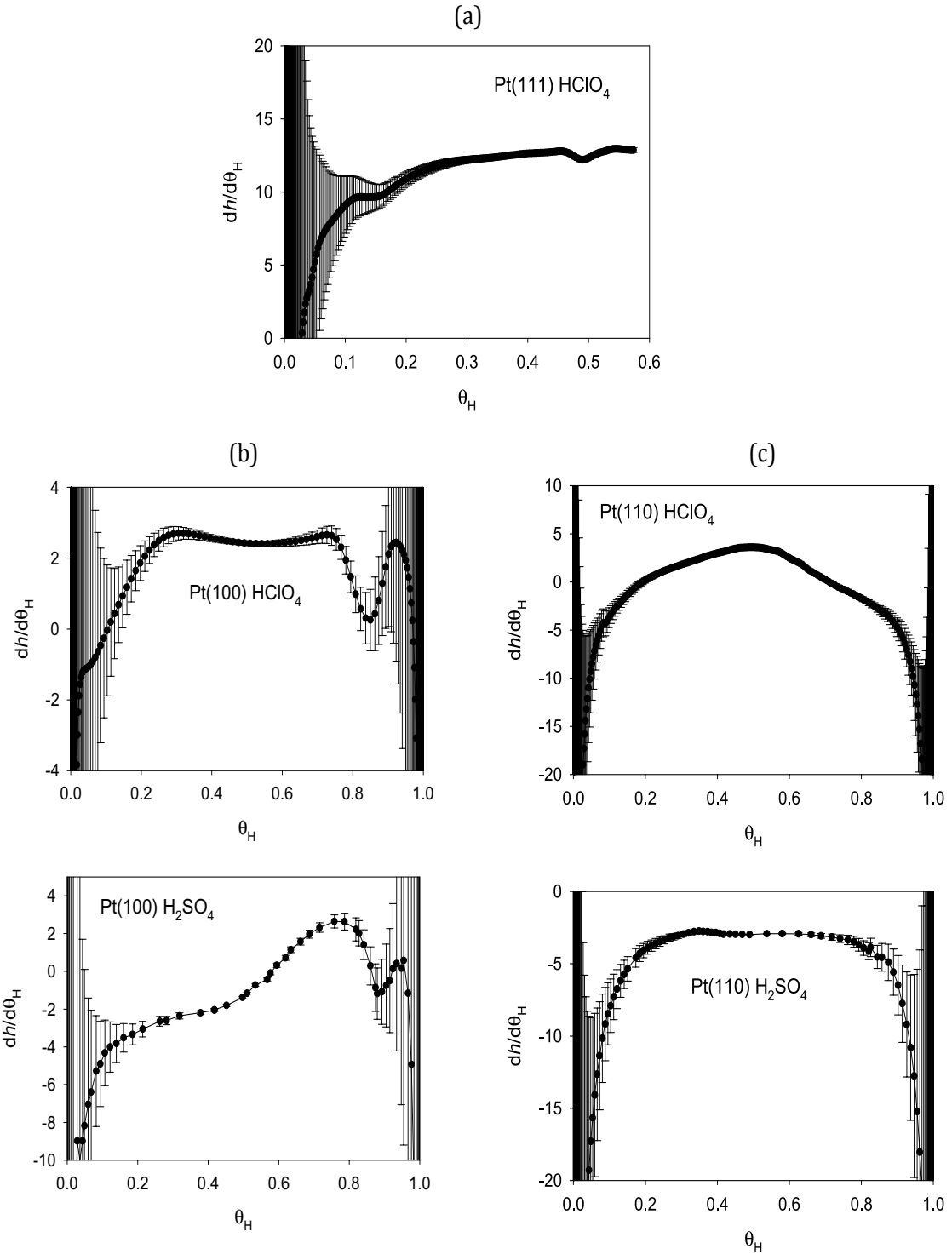

Figure 2.5: Dependence of $dh/d\Theta_H$ on Θ_H on (a) Pt(111), (b) Pt(100) and (c) Pt(110) [14].

Chapter 3

Calculation Methods

3.1 Density Functional Theory Calculation Method

All calculations were performed using the linear combination of atomic orbitals (LCAO) and pseudopotential scheme implemented in SIESTA (Spanish Initiative for Electronic Simulations with Thousands of Atoms) [54, 55] and the plane wave and projector augmented wave (PAW) potentials [56, 57] scheme implemented in VASP (Vienna Ab initio Software Package) [58, 59, 60] softwares. In the DFT calculation, we used the generalized gradient approximation (GGA) to the exchange-correlation functional due to Perdew, Burke, and Ernzerhof (PBE) [61]. The surface irreducible Brillouin zone was sampled on the k-point mesh generated by the Monkhorst-Pack (MP) scheme [62].

Part of the calculation was done using the Institute of Solid State Physics (ISSP) Super Computer Center. The amount of time for which a central processing unit (CPU time) was used for processing instructions of a computer program with 64 total cores is $\sim$ 1500000 seconds for equilibrating (1$\times$1) unit cell Pt system.

3.1.1 SIESTA calculation

The SIESTA calculation, which has been successfully applied to many researches on the metal surfaces, implements density functional theory within periodic boundary conditions. The mesh-cutoff of 200 Ry, the double-zeta polarized (DZP) basic set were used. We employed the Methfessel-Paxton function with the electronic temperature of 300 K in carrying out the Brillouin zone integrations. Within the SIESTA code the cutoff radius per angular momentum channel was determined by a parameter, the energy shift. In this work the energy shift was taken as 200 meV.

As an initial step, the surface and the molecule were treated as separate systems. For the Pt system, after running optimization, a GGA optimized lattice constant of Pt surface was determined. An isolated H_2 molecule was placed in the cubic unit cell of $\sim$ 7.5 Å and it was confirmed that the molecule does not interact with its periodic image using the spin polarized calculation. In the next step, the Pt atoms in the bottom layer were fixed and all other Pt atoms were relaxed, and the hydrogen atoms were placed on the binding sites of the Pt surfaces with the surface coverage from 0ML to 1ML. Then all configurations were relaxed again, both in the spin-polarized calculations and in the spin-unpolarized calculations, to obtain the optimized Pt-H bond lengths and the total energies.

3.1.2 VASP calculation

In the VASP calculation, the plane wave cutoff energy was set at 400 eV, which is sufficient to converge the total energy to values of the order of 1 meV per atom. Brillouin zone integrations were carried out by employing the Gaussian method with a smearing width of 0.02 eV. Structural relaxations were performed to account for the effects of surface relaxations. The procedure to determine the surface structure was similar to the one adopted in the SIESTA calculation.

3.2 Zero Point Energy Calculation

It is well known that the quantum effects are stronger for H than other elements and the effects cannot be neglected in many cases. The zero-point energy (ZPE) correction plays an important role in determining the adsorption site on metal surface where the potential surface is generally quite flat. However, ZPE has been sometimes neglected in the previous studies of H on the Pt surface [21, 25]. In this work, the ZPE of H on the Pt surface was found by changing the position of hydrogen atom around equilibrium position, i.e., we let hydrogen atom vibrate around the equilibrium position on the Pt surface.

The zero point energies of H on Pt surface were calculated by using:

$$\mathrm{ZPE} = \frac{1}{2}\hbar\omega, \tag{3.1}$$

where ω is corresponding phonon frequencies.

To calculate the phonon frequencies at the Γ point in the surface Brillouin zone, we used the forces associated with the displacements of the atoms in the supercell. From the forces obtained by the use of the Hellmann-Feynman theorem [63, 64], the elements of the force-constant matrix were calculated. Then the dynamical matrix was determined by a Fourier transformation, and the phonon frequencies for arbitrary wave vectors were evaluated by a diagonalization of this matrix. In our calculations, the periodically arranged supercells (3×3) for Pt(111) and (3×2) for Pt(110) were used. We displaced an atom i in the supercell along a small displacement vector $\vec{u}(i) = \{u_\alpha(i)\}$, where α is the Cartesian component. From the Hellmann-Feynman forces, $\vec{F}(i') = \{F_\alpha(i')\}$, we can determine one column of the force-constant matrix:

$$\phi_{\alpha\alpha'}(i,i') = -\frac{\partial F_{\alpha'}(i')}{\partial u_\alpha(i)} \approx -\frac{F_{\alpha'}(i')}{u_\alpha(i)}. \tag{3.2}$$

To find all components in the force-constant matrix for the H atoms on the Pt surface, we followed two steps:(i) all the H atoms were displaced in the x, y, and z directions to find the forces $F_\alpha(i')$, (ii) these forces were applied with a linear regression technique to find the force-constant matrix components. We confirmed that the forces are a linear function of the force-constant matrix components. However when $F_\alpha(i') \leq 10^{-3}\mathrm{eV/\AA}$ the linear dependence between $\phi_{\alpha\alpha'}(i,i')$ and $F_\alpha(i')$ was not clear,

but the numerical uncertainty thereby yielded will not affect the phonon frequency so much. With the force-constant matrix $\phi(i,i')$ the dynamical matrix at the Γ point in the surface Brillouin zone,

$$D_{\alpha\alpha'} = \sum_{i'} \frac{\phi_{\alpha\alpha'}(i,i')}{\sqrt{m_i m_{i'}}}, \tag{3.3}$$

is obtained, where m is the atomic mass. The diagonalization of $D_{\alpha\alpha'}$ then yields the phonon frequencies.

3.3 Monte Carlo Method

The main target of this study is to compute the thermodynamic properties of the surface, such as the adsorption free-energy and the effective H-H interaction. The DFT calculation is, however, too time-consuming to directly obtain those value. Instead, the total-energies obtained by the DFT calculations were fitted to a lattice model and the Monte Carlo simulation was done using the lattice gas model. Detail of the Monte Carlo simulation is described in this section.

We use the Monte Carlo (MC) simulation to accurately investigate the thermodynamic and properties of a system of interest. The average value of some property, $\langle A \rangle$ can be obtained as [65]:

$$\langle A \rangle = \frac{\int dr^N \exp\left[-\frac{1}{k_B T} U\left(r^N\right)\right] A\left(r^N\right)}{\int dr^N \exp\left[-\frac{1}{k_B T} U\left(r^N\right)\right]}, \tag{3.4}$$

where r^N is the configuration of an N particle system (i.e., the positions of all N particles) , U is the potential energy. The probability density of finding the system in configuration r^N is:

$$\rho(r^N) = \frac{\exp\left[-\frac{1}{k_B T} U\left(r^N\right)\right]}{\int dr^N \exp\left[-\frac{1}{k_B T} U\left(r^N\right)\right]}, \tag{3.5}$$

where $\int dr^N \exp\left[-\frac{1}{k_B T} U\left(r^N\right)\right]$ is the configurational integral. In Eq. (3.5), if the points of the sufficient number N_{MC} of MC steps can be randomly generated in configuration space, then we can write Eq. (3.4) in the form:

$$\langle A \rangle \approx \frac{1}{N_{\mathrm{MC}}} \sum_{i=1}^{N_{\mathrm{MC}}} A\left(r_i^N\right). \tag{3.6}$$

The errors in $\langle A \rangle$ will be $1/\sqrt{N_{\mathrm{MC}}}$ after equilibration of our system of interest [65].

A MC algorithm contains a group of Monte Carlo moves that generates a Markov chain of states. It means that if we consider our system is currently in state m, then the probability of moving to a state n is defined as π_{mn}, where π is the transition matrix. Consider ρ is a probability vector, that defines the probability

that the system is in a particular state; ρ_i is the probability of being in state i. For the simulation to converge to the limiting distribution, the Monte Carlo moves used must satisfy the balance condition and they must result in ergodic sampling [66]. It means that the net flux between two states must be zero at equilibrium, i.e.:

$$\rho_m \pi_{mn} = \rho_n \pi_{mn}. \tag{3.7}$$

For proposing a Monte Carlo move and correctly choose whether to accept or reject it, the Metropolis acceptance criterion [67, 68] was used:

$$p_{mn} = \min\{1, \exp(-\beta[U(n) - U(m)])\}, \tag{3.8}$$

where p_{mn} is the probability of accepting the move. If $U(n) > U(m)$, a pseudorandom number U_{pseudo} $(0 < U_{pseudo} < 1)$ will be generated. If $U_{pseudo} < p_{mn}$, the trial move is accepted.

Chapter 4

The Pt(111)

This chapter has been published as :

"First-Principles Thermodynamic Description of Hydrogen Electroadsorption on the Pt(111) Surface"

by T.T.T. Hanh, Y. Takimoto, O. Sugino, Surf. Sci. 625 (2014) 104.

4.1 Introduction

The hydrogen (H) adsorption is one of the most widely studied issues in surface science for many years [39, 69]. Because of many applications, the adsorption on platinum (Pt) surfaces has been paid special attention either under the ultra-high vacuum (UHV) [70, 71] or in contact with the solution [7, 8, 9, 10, 11, 72, 73, 74, 75]. This issue, especially H on Pt(111), has been the target of many theoretical calculations [15, 16, 17, 18, 19, 20, 21, 22, 23, 24, 25, 76, 77]. Earlier theoretical studies focused on the UHV surface [15, 16, 17, 18, 19, 20, 21, 22, 76], and more recent ones [23, 24, 25] modeled the electrochemical interfaces with the UHV surface neglecting the hydration effect. Understanding of the hydration effect is a challenging theme itself, but it is a practical first step to compare in detail the UHV surface calculation with the electrochemical experiment. To proceed the study along this line, however, the data provided by previous theoretical studies is still insufficient, and at this stage, it is important to provide more theoretical data to precisely understand the difference and/or similarity between the theory and experiment.

As a tool to investigate the surfaces in UHV, the first-principles calculation has shown great success. In the case of the surfaces in UHV, one can use the surface structures determined experimentally or those optimized within the theory to investigate the properties of the surface. In the case of the solid/liquid interface, however, things are different. The liquid structures fluctuate rapidly and the theory needs to deal with the statistics of the liquid structures. This is a heavy burden of the calculation and it is still infeasible to take it fully into account. Instead, the UHV surface approach has been applied to the problem of *hydrophobic* interfaces where interaction with the solution is weak. The approach has been considered valid for platinum or other noble metal and large number of calculations can be found in the literatures [12, 13].

Experimentally, the H adsorption isotherm has been traditionally studied using the cyclic voltammetry (CV) [7, 8, 9, 10, 11]. From the current-voltage curve, the amount of adsorbed H atoms (H_{ads}) can be obtained as a function of the bias potential (U) because $H_3O^+ + e^- \leftrightarrow H_{ads} + H_2O$ is the only major charge transfer process concerned. The H-coverage (Θ_H) is found sensitively dependent on the Pt-H binding energy and the H-H interaction energy, so that the $\Theta_H(U)$ curve is a fingerprint of the surface. For example, recent experiment [14] showed that the effective H-H interaction is strongly repulsive on Pt(111) in a $HClO_4$ solution, while the interaction is much weakened both on Pt(100) and Pt(110), and the interaction becomes attractive when in a H_2SO_4 solution. The electrochemical measurement, however, does not provide detail on the adsorption site. The spectroscopic measurement can in principle provide it in a complementary way, but the measurement has not been somehow conclusive. In this context, it was deduced so far, and is generally believed, that the hollow site is the most stable site although some spectroscopic data suggests adsorption on the top site, leaving room for controversy [8].

In this context, it is important to perform the first-principles density functional theory (DFT) calculation to obtain the thermodynamic adsorption energy. The previous calculations [76, 15, 16, 17, 18, 19, 20, 21, 22, 23, 24, 25], however, did not lead to the same conclusion regarding the most stable adsorption site. This happened despite the fact that those calculations commonly used the semilocal level of the Kohn-Sham theory, *i.e.*, the generalized gradient approximation (GGA) for the exchange-correlation of the electrons. Olsen *et al.* [15] used the linear combination of atomic orbital (LCAO) scheme to find that the top site is more stable than the fcc site (the next stable site) by 110 meV when $\Theta_H = 1/4$. Later, plane wave basis set was used under $\Theta_H = 1/4$ to find that (1) the adsorption energy is almost identical among the top, fcc, hcp, and a site between the fcc and bridge by Nobuhara *et al.* [16], similarly that (2) the top is more stable than the fcc by only 10 meV by Ford *et al.* [21], but that (3) the top is more stable than the bridge (the next stable site) by 900 meV by Watson *et al.* [17], and that (4) the fcc is more stable than the top by 60 meV by Greely *et al.* [22]. Bădescu *et al.* [18] did a similar calculation under $\Theta_H = 1$, and found that the top is more stable than fcc (the next stable site) by 22 meV when H is treated classically, but the fcc becomes more stable than the top by 21 meV when corrected by the zero point energy (ZPE), suggesting importance of the zero point energy. Hamada *et al.* [25] also did a similar calculation under various coverage conditions to find that the fcc is more stable than the top by 40 meV without the ZPE correction under $\Theta_H = 1/4$ in consistent with Ref. [22], but the adsorption energy was shown to have significant layer thickness dependence and one needs to use more than 9 Pt layers to get a converged result, which is thicker than those adopted in previous calculations. These qualitatively different results obtained by the previous studies suggest that more careful DFT calculation needs to be done to conclude the stability among the possible adsorption sites. In this context, obtaining a converged DFT data is the first topic that we discuss in this chapter.

We will then compute the adsorption isotherm and compare the result with those obtained from the CV measurement [10, 11, 14]. We will focus on the comparison of the effective H-H interaction, or the g-value, using a Monte Carlo simulation

on a lattice gas model parameterized by the results of the DFT calculations. Note that a similar Monte Carlo simulation was done by Karlberg *et al.* [23] using the fcc site only to compare the theoretical and experimental isotherm, $\Theta_{\mathrm{H}}(U)$, but here we use both the fcc and the top sites and compare the derivative of the isotherm, which corresponds to the g-value. This is the second topic of this chapter. We examine if the lattice gas model successfully accounts for the experiment or it needs adjustment of the parameters. Discrepancy from the experiment should be ascribed to the hydration effect and/or the DFT-GGA error albeit it is not possible to discuss relative importance. The comparison nevertheless provides important insight into the H-adsorption, which prompts further theoretical investigation.

4.2 Density Functional Theory (DFT) calculations

4.2.1 Computational methods

We used the linear combination of atomic orbitals (LCAO) and pseudopotential scheme implemented in SIESTA (Spanish Initiative for Electronic Simulations with Thousands of Atoms) [54, 55] for most of the first-principles electronic structure calculations, while some of the results were corrected using the plane wave and projector augmented wave (PAW) potentials [56, 57] scheme implemented in VASP (Vienna Ab initio Software Package) [58, 59, 60]. The models and some detail of the DFT calculation used for the calculation are shown in Fig. 4.1. In the DFT calculation, we used the generalized gradient approximation (GGA) to the exchange-correlation functional due to Perdew, Burke, and Ernzerhof (PBE) [61]. The repeated slab model was used to model the surface and the surface slab was separated from its periodic image by 13.6 Å, by which interaction energy with the image can be reduced to 1 meV. The surface irreducible Brillouin zone was sampled on the k-point mesh generated by the Monkhorst-Pack (MP) scheme[62].

SIESTA calculation

The SIESTA calculation was done using standard computational parameters, which provided reasonably accuracy both in the calculation of a bare Pt surface and a Pt molecule. We have adopted the following computational parameters for the SIESTA calculation. We used the double-zeta polarized (DZP) basic set, the mesh-cutoff of 200Ry. We employed the Fermi-Dirac function with the electronic temperature of 300K in carrying out the Brillouin zone integrations. We used the value 200 meV for the energy shift for Pt, which determines the cutoff radius per angular momentum channel. For adsorbed H atoms, more extended basis was used; we used the value 60 meV for the energy shift, and split norm of 0.53 for the second zeta. This ensure to obtain correct bond length and energy of H_2 molecule, and is important for the long range interactions. The optimized lattice constant of the bare Pt(111) is 3.9247 Å in good agreement with the experimental bulk lattice constant (3.9242 Å) [78].

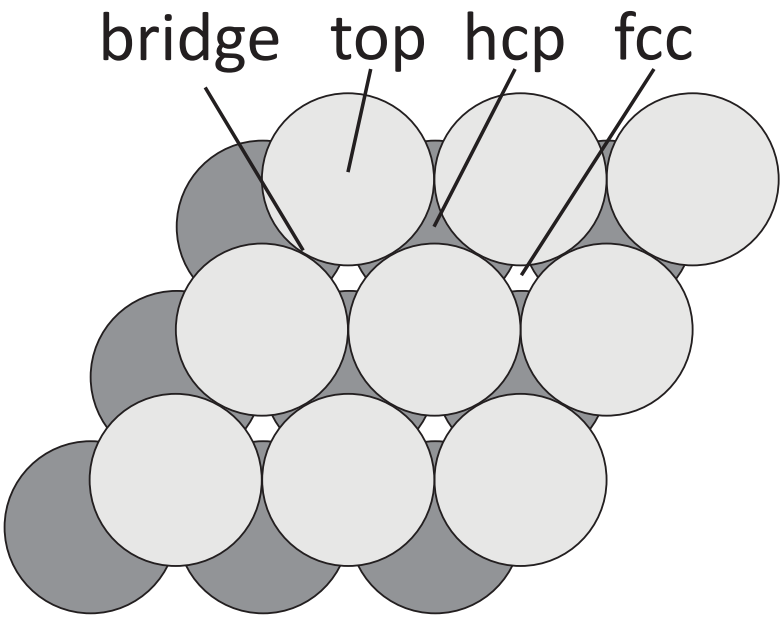

Figure 4.1: The Pt(111) model used for the DFT calculations. The surface was modeled using the repeated slab model. In the SIESTA calculation, the (1×1), (2×2), (3×3), and (4×4) lateral unit cells were used to construct the Pt(111) slabs, on which H atoms were adsorbed on the top, fcc, hcp, and bridge site such that the coverage ranges from zero to one; the above figure corresponds to (2×2). The VASP calculation was done only for (1×1) with only one H adsorbed either on the top or the fcc. A vacuum equivalent to a six-layer slab separated the Pt slabs, where the interlayer spacing was taken as 2.27 Å. The total energy was obtained after relaxing all the H and Pt atoms except for the bottom two Pt-layers.

The equilibrium bond length (l_{eq}) and the binding energy (E_b) of an isolated H_2 molecule were obtained by using the cube unit cell of length ∼7.5 Å and by allowing spin polarization. The result, $l_{eq} = 0.754$ Å and $E_b = 4.525$ eV, is in good agreement with experimental data, $l_{eq} = 0.74$ Å and $E_b = 4.530$ eV [79]. The zero point energy (ZPE) is 0.269 eV, in agreement with textbook data 0.270 eV [80].

The calculation of the H adsorbing surfaces was done for the following four sets of configurations. First, one H atom was adsorbed on the surfaces of (1×1), (2×2), and (3×3) lateral unit cell. This calculation was done mainly for the sake of comparison with previous calculation. Second, the surface of (1×1) lateral unit cell was used to investigate convergence property with respect to the number of Pt layers and the *k*-point mesh. Third, the surface of (3×3) lateral unit cell and four Pt layers were used to let H atoms adsorb on the top, fcc, hcp, and bridge under sub-monolayer coverage conditions, *i.e.*, $\Theta_H \leq 1$. Fourth, two H atoms were let adsorb on the (4×4) lateral unit cell to do the calculation with the (2×2×1) MP grids to investigate the H-H interaction.

In the third case, all possible configurations were generated and the calculated total-energies were fitted to a lattice gas model as detailed below. There were some configurations that showed appreciable relaxation from the symmetric position, which were omitted in the fitting. In this case, we used both the spin-polarization and unpolarization calculations although spin was unpolarized in other cases. In the Brillouin zone integration, 28, 15 and 6 special *k*-points were used to sample the (7×7×1), (5×5×1) and (3×3×1) MP grids for the (1×1), (2×2), and (3×3) lateral unit cells, respectively. The zero point energy (ZPE) of H was calculated by displacing the position of H around equilibrium position both in the surface normal and surface parallel directions and by using a harmonic approximation. The ZPE calculation was done using those configurations adsorbed on the same symmetric sites, *i.e.*, the top or the fcc, only.

VAPS calculation

The VASP calculation was done only for (1×1) with only one H adsorbed on the surface. We have used the *k*-point mesh ranging from (8×8×1) to (24×24×1) MP grids for the (1×1) lateral unit cell. We have used the following computational parameters. The plane wave cutoff energy was 400 eV, which is large enough to converge the total energy within the order of 1 meV per atom. Brillouin zone integrations were carried out by employing the Gaussian smearing function with width 0.02 eV.

4.2.2 DFT-GGA description of H on Pt(111)

Comparison with previous calculations

We begin by showing that the properties except for the adsorption energy have rapid convergence with respect to the computational parameters, and correspondingly the results agrees well with previous calculations. First, we compare the optimized Pt-H bond lengths for the H on Pt(111) as shown in Table 4.1, showing good agreement

cell	Pt layers	top	bridge	fcc	hcp
			1 ML		
(1×1)	4	1.57	1.78	1.87	1.88
	5	(1.55)	(1.76)	(1.85)	(1.85)
			1/4 ML		
(2×2)	4	1.57	1.78	1.89, 1.89, 1.89	1.89, 1.89, 1.89
	5	(1.55)	(1.75)	(1.85, 1.85, 1.85)	(1.86)
			1/9 ML		
(3×3)	4	1.57	1.78	1.88, 1.88, 1.88	1.88, 1.88, 1.88

Table 4.1: The optimized Pt-H bond length (Å). The results from Ref. [25] are parenthesized.

with the values of Hamada *et al.* [25]. We have confirmed that the results were affected by less than 1 % when changing the number of Pt layers from four to five. From the calculation we found that the H atoms are kept almost at the ideal high symmetry position.

Second, we compare the vibrational frequency and zero point energy (ZPE). Using the supercell approximation, the phonon frequency was obtained for the H adsorption configurations on the (3×3) lateral unit cell. The obtained frequency for H_{fcc} under the full monolayer coverage is 80.9 cm^{-1} for the surface parallel component (P) and 145.0 cm^{-1} for the surface vertical component (V), which agrees well with the previous calculation (73.5 cm^{-1} for P and 142.6 cm^{-1} for V) [81]. The zero point energies estimated from the calculated frequency are 40.5 meV (P) and 72.5 meV (V), which agree fairly well with the UHV experiment for the vertical component, but discrepancy is not small for the parallel (62.1±6.0 meV (P) and 80.8±3.9 meV (V) [82]. The result for the top is 53.0 cm^{-1} for P and 272.4 cm^{-1} for V in agreement with the previous calculation (47.4 cm^{-1} for P and 277.2 cm^{-1} for V) [81].

The stretching frequencies of H on the top are listed in Table 4.2, which show good agreement with the values of previous DFT calculations [18, 19, 21, 25]. Also, $\nu_{H\text{-}Pt}$ for top sites of ∼2100 cm^{-1} and $\nu_{Pt\text{-}H}$ for hollow sites of ∼1100 cm^{-1} are quite close to the experimental values [75]. The averaged ZPE's of H on the top and the fcc were calculated using only the (1×1) lateral cell because of limited capacity of our computer. The results are ∼182 meV and ∼134 meV, respectively, for the top and the fcc, which agree with the results of Källén *et al.* (190 meV for the top and 139 meV for the fcc) [84]. (For the meaning of "average" please read the following subsection.)

H-adsorption energy

Table 4.3 shows the adsorption energy of H calculated using

$$E_{ads} = E_{tot}(N_H) - E_{tot}(0) - \frac{n_H}{2} E_{H_2},$$

cell	Pt layers	top	bridge	fcc	hcp
		1 ML			
(1×1)	3	2175	1373	1159	1178
	4	2180	1349	1150	1189
	5	2192	1363	1184	1219
		1/4 ML			
(2×2)	3	2171	1314	1107	1138
	4	2167	1338	1070	1126
	5	2187	1335	1095	1114
		1/9 ML			
(3×3)	4	2167	1323	1065	1185

Table 4.2: The Pt-H stretching frequency (cm^{-1}).

where $E_{\mathrm{tot}}(N_{\mathrm{H}})$ is the total energy of the Pt surface adsorbed with N_{H} H atoms and E_{H_2} is the total energy of the isolated H_2 molecule. E_{ads} shows significant coverage dependence, indicating H-H interaction plays a role; the interaction will be analyzed in the following subsection. It is worth emphasizing that the calculated value depends on the number of Pt layers, indicating that convergence is not reached yet when using the 4-layed slab. In this respect, the result agrees with the conclusion of Hamada *et al.* [25]. To obtain the converged value, we now investigate in detail the convergence property with respect to the number of Pt layers and k-points.

The calculation was done using (1×1) lateral unit cell, on which one H atom was let adsorb either on the top or on the fcc. The convergent was investigated only for on-site energy, without including the H-H interaction for (1×1) lateral unit cell because this converged result, then, will be used to correct the adsorption energy of not converged (3×3) unit cell system, in which the H-H interaction of one H atom adsorbed on the surface is considered vanishing. Table 4.4 shows the calculated adsorption energy and Fig. 4.2 plots the adsorption energy on the fcc relative to that on the top, ΔE_{ads}. The table shows that the SIESTA calculation provides the adsorption energy systematically larger by 0.1 eV in magnitude when compared with the VASP calculation. The figure shows that they provide a similar dependence on k-point mesh and number of Pt layers as it changes from (8×8×1) to (12×12×1) MP grids and from three to ten layers. In the following, we will focus on the relative energy only, which is relevant to the issue of the relative abundance. The value oscillates with large amplitude, indicating that the number of layers and k-points should be made larger to obtain the converged value. Further calculation was done using VASP only, which was found to more efficiently diminish the charge sloshing that hampers stable calculation of thick metallic slabs. Fig. 4.3 plots the results obtained with (12×12×1) MP grid, which is oscillatory against the number of layers but the oscillation is regular and periodic when taking 14 to 18 layers. It suggests that the converged value has already been determined well within the amplitude of the oscillation (∼10 meV) by taking these layers. Fig. 4.4 plots the dependence on k-points, which shows that the results for various number of Pt layers (14-17) becomes very close to each other when using (24×24×1) MP grid. From these results we conclude that the converged ΔE_{ads} is located at around -7

cell	Pt layers	top	bridge	fcc	hcp
			1 ML		
(1×1)	3	−0.461	−0.390	−0.432	−0.405
		(−0.487)	(−0.450)	(−0.519)	(−0.474)
	4	−0.464	−0.384	−0.432	−0.402
		(−0.336)	(−0.338)	(−0.434)	(−0.378)
	5	−0.567	−0.489	−0.527	−0.499
		(−0.444)	(−0.399)	(−0.467)	(−0.420)
			1/4 ML		
(2×2)	3	−0.719	−0.608	−0.601	−0.589
		(−0.567)	(−0.522)	(−0.522)	(−0.516)
	4	−0.646	−0.547	−0.563	−0.507
		(−0.411)	(−0.461)	(−0.518)	(−0.454)
	5	−0.682	−0.565	−0.578	−0.537
		(−0.518)	(−0.500)	(−0.568)	(−0.493)
			1/9 ML		
(3×3)	4	−0.656	−0.576	−0.612	−0.524

Table 4.3: The adsorption energy of H (eV). The results from Ref. [25] are parenthesized.

Pt layers	(8×8×1)MP		(9×9×1)MP		(10×10×1)MP		(11×11×1)MP		(12×12×1)MP	
	top	fcc	top	fcc	top	fcc	top	fcc	top	fcc
3	−0.56	−0.55	−0.59	−0.53	−0.57	−0.54	−0.57	−0.54	−0.59	−0.56
	(−0.41)	(−0.40)	(−0.44)	(−0.38)	(−0.42)	(−0.39)	(−0.43)	(−0.40)	(−0.45)	(−0.41)
4	−0.49	−0.54	−0.49	−0.53	−0.49	−0.49	−0.52	−0.54	−0.48	−0.5
	(−0.34)	(−0.39)	(−0.33)	(−0.36)	(−0.34)	(−0.34)	(−0.36)	(−0.38)	(−0.32)	(−0.34)
5	−0.56	−0.58	−0.62	−0.57	−0.51	−0.49	−0.57	−0.54	−0.59	−0.54
	(−0.42)	(−0.43)	(−0.46)	(−0.43)	(−0.36)	(−0.35)	(−0.43)	(−0.39)	(−0.44)	(−0.39)
6	−0.52	−0.55	−0.53	−0.53	−0.49	−0.49	−0.55	−0.55	−0.53	−0.53
	(−0.38)	(−0.42)	(−0.38)	(−0.39)	(−0.35)	(−0.36)	(−0.40)	(−0.40)	(−0.38)	(−0.39)
7	−0.64	−0.61	−0.55	−0.53	−0.50	−0.47	−0.55	−0.53	−0.57	−0.53
	(−0.35)	(−0.38)	(−0.41)	(−0.38)	(−0.36)	(−0.34)	(−0.42)	(−0.40)	(−0.43)	(−0.39)
8	−0.56	−0.58	−0.57	−0.57	−0.48	−0.50	−0.53	−0.53	−0.52	−0.51
	(−0.42)	(−0.45)	(−0.43)	(−0.42)	(−0.36)	(−0.36)	(−0.39)	(−0.39)	(−0.38)	(−0.38)
9	−0.45	−0.51	−0.54	−0.50	−0.54	−0.52	−0.55	−0.56	−0.53	−0.50
	(−0.33)	(−0.37)	(−0.40)	(−0.35)	(−0.39)	(−0.38)	(−0.41)	(−0.42)	(−0.38)	(−0.36)
10	−0.57	−0.57	−0.58	−0.56	−0.48	−0.48	−0.53	−0.53	−0.56	−0.52
	(−0.43)	(−0.44)	(−0.43)	(−0.41)	(−0.35)	(−0.35)	(−0.41)	(−0.40)	(−0.42)	(−0.39)

Table 4.4: The adsorption energy of H (eV), using SIESTA calculation. The results from VASP calculation are parenthesized.

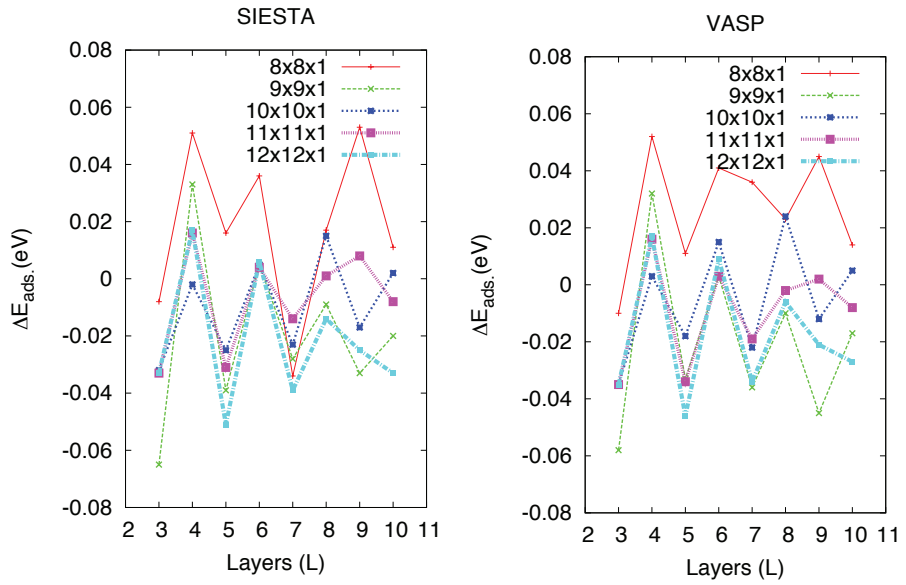

Figure 4.2: The relative adsorption energy, $E_{\text{ads}}(\text{top}) - E_{\text{ads}}(\text{fcc})$, calculated using SIESTA (left) and VASP (right).

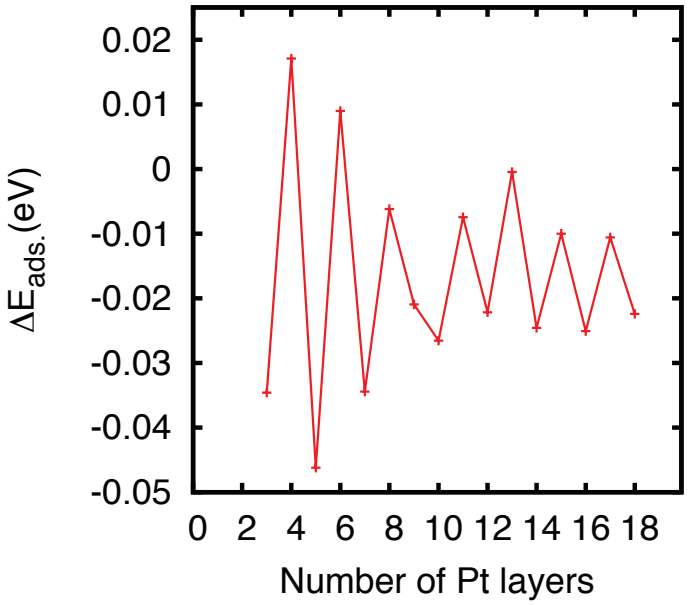

Figure 4.3: Pt layer thickness dependence of ΔE_{ads}.

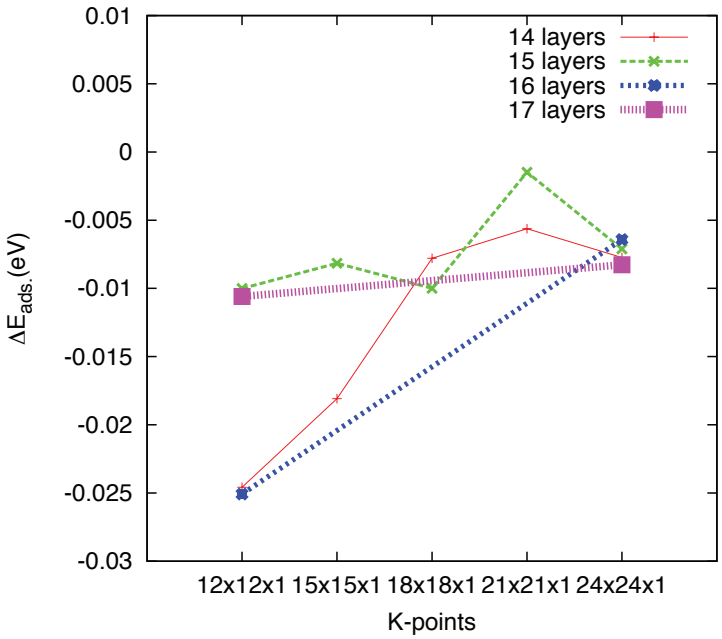

Figure 4.4: k-point dependence of ΔE_{ads}.

meV. When adding ZPE, the value becomes -55 meV, or the fcc is more stable by that amount, which is only two times the typical thermal energy at 300K (25 meV). This is our conclusion on the theoretical adsorption energy within the UHV surface and DFT-PBE. Besides, we have used a different functional called RPBE [83] for the calculation with (1×1) cell, 3-5 Pt layers, and $(9 \times 9 \times 1)$ MP grids. With RPBE, the adsorption energy on the fcc relative to that on the top was found systematically lowered by 20 meV. This functional effect is smaller than ZPE albeit not very much smaller than that, indicating that almost degenerated nature of the two sites is common to both cases. We will examine below if this will naturally explain the CV measurement. In doing the investigation thermodynamically, we use the non-converged value of E_{ads} obtained by using the four layer slab calculation and then correct the fitted data by shifting up the on-site energy of the top relative to that of the fcc by 25 meV afterwards. This means that we assume (without justification) that the correction (25 meV) is common to all the configurations with different coverage. This approximated treatment is motivated by the finding that, when comparing ΔE_{ads} at 1/4 ML condition, the dependence on the number of Pt layer looks similar in the 3-5 layers region (Fig. 4.5).

Mapping to a lattice gas model

Out of all possible H-adsorptions on the (3×3) lateral unit cell using (3×3×1) MP grid, 123 configurations showed minor displacement from the symmetric position (*i.e.*, the top, fcc, hcp, or bridge). The results were then fitted to a lattice gas model of the form,

$$H = \sum_{\alpha} \varepsilon_{\alpha} n_{\alpha} + \sum_{\alpha\beta} v_{\alpha\beta} n_{\alpha} n_{\beta},$$

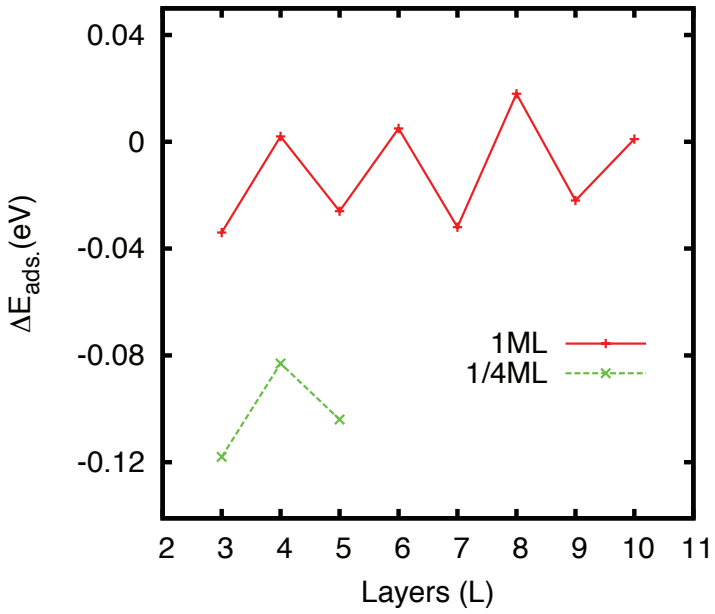

Figure 4.5: ΔE_{ads} for different coverage conditions.

site	(spin-unpolarized)	(spin-polarized)
top	$-0.657(-0.475)$	$-0.657(-0.475)$
fcc	$-0.612(-0.478)$	$-0.619(-0.485)$
hcp	-0.524	-0.526
bridge	-0.576	-0.576

Table 4.5: The fitted on-site energy (eV). The data corrected with ZPE is shown in parenthesis.

where ε_α is the on-site energy for $\alpha \in \{\text{top, fcc, hcp, bridge}\}$ and $v_{\alpha\beta}$ is the pairwise interaction energy. Those pairs with distance less than 2.42 Å were omitted by assigning infinite energy, and among those with larger distance, the smallest one were assigned finite value and others were assigned zero. Only for the top-top and bridge-bridge pair, however, finite values were assigned up to the next nearest pairs. Under these constraints, the total energies of SIESTA were fitted using the standard regression algorithm. Resulting values are listed in Tables 4.5 and 4.6. The mean error of the fitting is $\sim$17 meV and the maximum error is $\sim$51 meV. Although we have analyzed four kinds of site, the hcp and the bridge sites have larger value for the on-site energy than do the top and the fcc, yielding much less probability for the occupation. In this context, we will focus only on the top and the fcc hereafter.

The zero point energy (ZPE) was fitted independently as follows. ZPE was calculated by diagonalizing the dynamical matrix as stated above for all the configurations adsorbed at the top sites or the fcc only; the results were subsequently averaged over the configurations of the same coverage to get $E_{\mathrm{ZPE}}(\Theta_{\mathrm{H}})$. The coverage dependence is almost linear except for the low coverage region ($\Theta_{\mathrm{H}} < 0.2$) where the deviation from the linearity is 5-10 meV. The linear dependence on the

site	top	fcc	hcp	bridge
top	0.049, 0.0114	0.028	0.035	0.112
	(0.049, 0.0114)	(0.029)	(0.036)	(0.113)
fcc		0.028	0.013	0.144
		(0.028)	(0.014)	(0.146)
hcp			0.023	0.158
			(0.023)	(0.159)
bridge				0.078, 0.046
				(0.078, 0.044)

Table 4.6: The fitted interaction energy (eV) obtained from spin-unpolarized calculation. The data obtained from spin-polarized calculation is parenthesized.

H-H pair	energy		
H_{fcc}-H_{fcc}	0.027 (0.031)	0.011 (0.011)	0.004 (0.000)
H_{top}-H_{top}	0.037 (0.042)	0.020 (0.020)	0.005 (0.000)
H_{fcc}-H_{top}	0.027 (0.027)	0.019 (0.000)	-

Table 4.7: The long-range interaction parameters (eV) for the lattice gas model. The values in parenthesis are the original (short-range) parameters. The first, second, and third rows indicate the first, second and third H neighbours, respectively.

coverage indicates local nature (and thus additive nature) of the zero point energy. The averaged ZPE energy was then used to correct the on-site energy (Table 4.5).

To check the accuracy of the mapping, we did further calculations. We performed SIESTA calculations using (4×4) lateral unit cell and 4 special *k*-points in the (2×2×1) MP grid. We have taken even number for the MP grid in this case to make the grid density almost equal to the one used in our (3 × 3) cell calculation, although odd/even oscillation may affect the result. The result shows that the energy required to subtract certain H_{fcc}-H_{fcc} pairs are 15 meV and 7 meV for (4×4) while the values are 12 meV and 1 meV for (3×3), respectively, indicating that the effect of the lateral cell size is not so large. As another check, we fitted the total energy using (3×3) lateral unit cell in the above using larger number of parameters, so that longer-range interaction can be included. The resulting interaction parameters, which we call long-range interaction parameters, are shown in Table 4.7 and Fig. 4.6 and are compared with the original parameters parenthesized in the same table, which we call short-range interaction parameters. Those parameters are found close to each other, and for those pairs outside the range of the short-range interaction parameter, the value is less than ∼20 meV, which is comparable to the mean error of the fitting (17 meV).

It is interesting to note that the almost degenerated nature between the top and the fcc is not the common feature of noble metal surfaces: Indeed, for Ir(111) surface [85] and Pd overlayers with (111) texture [86] the top is the most stable.

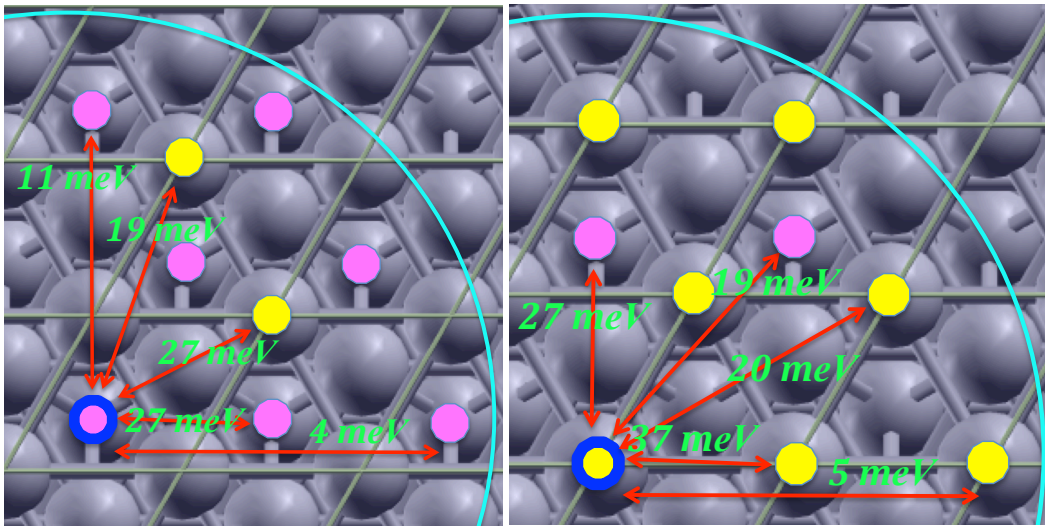

Figure 4.6: The interaction parameters. Those H atoms located within the cut-off radius (shown with a quarter of circle) from H_{fcc} (left panel) and H_{top} (right panel) are taken into account for the parameter fitting. The H-H pair and the interaction energy are shown in the figure.

4.3 Monte-Carlo (MC) simulation

4.3.1 Free-energy and effective H-H interaction

Having constructed the lattice gas model, we now perform the MC simulation to compute the free-energy of adsorption, which is used to evaluate the effective H-H interaction $V_{\text{H-H}}^{\text{eff}}$ and compare it with experiment in detail.

Using the fact that, for a system of strong repulsion, the H adsorption energy is rapidly increased with increase in the H coverage, the effective interaction will be defined as the coverage derivative of the adsorption energy. In that case, it will be natural to use for the adsorption energy the Gibbs free-energy, $G(N_{\text{H}},T)$, subtracted by the configurational entropic term, *i.e.*, to use the enthalpic term $G(N_{\text{H}},T)+TS_{\text{config}}(N_{\text{H}},T)$, with the reference free-energy taken to be $G(0,T)+\frac{1}{2}N_{\text{H}}\mu^0_{\text{H}_2}$, where $\mu^0_{\text{H}_2}$ is the chemical potential of hydrogen gas at standard condition. That is, the adsorption energy is

$$E^0_{\text{ads}}(N_{\text{H}},T)\equiv\left[\frac{\partial}{\partial N_{\text{H}}}\left\{G(N_{\text{H}},T)+TS_{\text{config}}(N_{\text{H}},T)-\frac{1}{2}N_{\text{H}}\mu^0_{\text{H}_2}\right\}\right]_T$$

or equivalently

$$E^0_{\text{ads}}(\Theta_{\text{H}},T)\equiv\left[\frac{1}{N_{\text{site}}}\frac{\partial}{\partial\Theta_{\text{H}}}\left\{G(\Theta_{\text{H}},T)+TS_{\text{config}}(\Theta_{\text{H}},T)\right\}\right]_T-\frac{1}{2}\mu^0_{\text{H}_2},$$

where $N_{\rm site}$ is the number of adsorption sites of the system. Then the effective interaction is

$$V^{\rm eff}_{\rm H\text{-}H}(\Theta_H, T) = \left(\frac{\partial E^0_{\rm ads}(\Theta_{\rm H}, T)}{\partial \Theta_H} \right)_T$$
$$= \left(\frac{1}{N_{\rm site}} \frac{\partial^2}{\partial \Theta^2_{\rm H}} \left\{ G(\Theta_{\rm H}, T) + TS_{\rm config}(\Theta_{\rm H}, T) \right\} \right)_T .$$

We will use its dimensionless parameter $V^{\rm eff}_{\rm H\text{-}H}(\Theta_{\rm H}, T)/(k_B T)$, which will be called as the g-value, or

$$\bar{g} \equiv V^{\rm eff}_{\rm H\text{-}H}(\Theta_{\rm H}, T)/(k_B T) \tag{4.1}$$

following Refs. [7, 8, 14]. Note that the g-value defined here is slightly different from the experimental one denoted as g, which is defined in Eq. (11) of Ref. [14]. The experimental one, g, is equivalent to the g-value obtained by substituting $S_{\rm config}(N_{\rm H}, T)$ with the *non-interacting* counterpart

$$S^{\rm n.i.}_{\rm config} = -N_{\rm site} k_B \left[\Theta_{\rm H} \ln \Theta_{\rm H} + (1 - \Theta_{\rm H}) \ln (1 - \Theta_{\rm H}) \right].$$

Therefore those g-values are different by the interaction contribution to the configurational entropy, $\Delta S \equiv S_{\rm config} - S^{\rm n.i.}_{\rm config}$, as

$$\bar{g} - g = \frac{1}{k_B N_{\rm site}} \frac{\partial^2 \Delta S}{\partial \Theta^2_{\rm H}}. \tag{4.2}$$

In computing the adsorption energy $E^0_{\rm ads}(\Theta_{\rm H}, T)$ and the entropy ΔS, we performed the MC simulation and the thermodynamic integration. The thermodynamics integration was done with respect to the interaction parameter λ, such that the thermal average of the λ-derivative of the parametrized lattice gas Hamiltonian,

$$H(\lambda) = \sum_\alpha \varepsilon_\alpha n_\alpha + \lambda \sum_{\alpha\beta} v_{\alpha\beta} n_\alpha n_\beta,$$

was integrated from $\lambda = 0$ (which corresponds to the non-interacting system) to $\lambda = 1$ (which corresponds to fully interacting system), to obtain the difference in the free-energy. The difference was used to obtain the difference in the entropy ΔS.

4.3.2 MC simulation conditions

The MC simulation was done at a given particle number $N_{\rm H}$ and the temperature T condition. Initially, the adsorbed H atoms were placed randomly at the allowed position. Due to the repulsive nature of the interaction, conventional Metropolis algorithm tends to be very slow in the configuration change, or the acceptance ratio is very low, when randomly choosing new H site. In order to increase the acceptance ratio, we have adopted Kawasaki-type dynamics where new site is chosen by the exchange of adsorbed H location to a neighboring empty one. The location is first selected by listing all allowed empty sites of non-zero pair interaction energy with respect to randomly selected occupied H site. Then, the new place is chosen

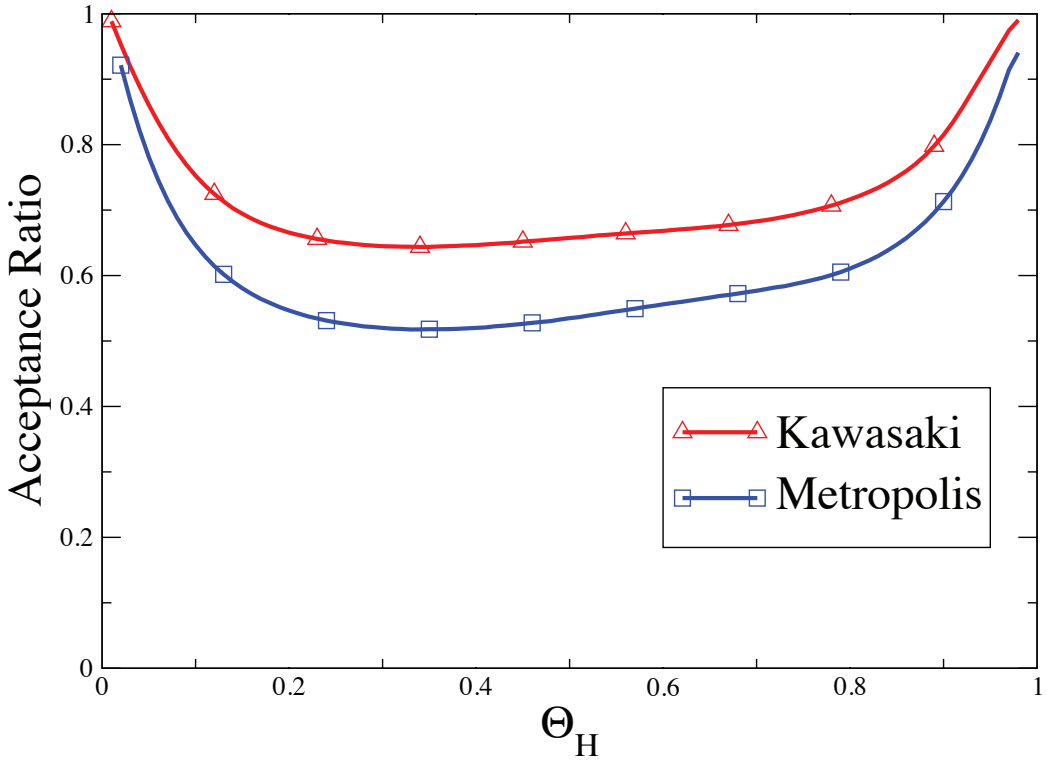

Figure 4.7: Acceptance ratio for the Kawasaki-type dynamics and for the original Metropolis dynamics.

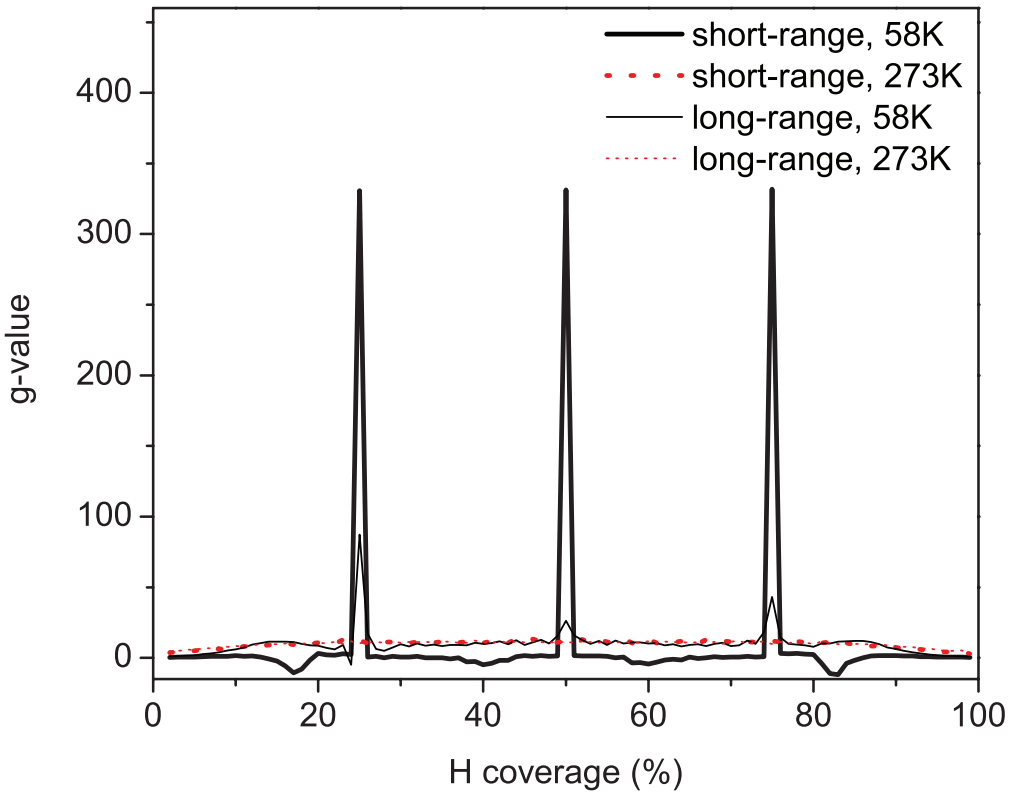

Figure 4.8: The calculated g-value obtained using the short-range interaction and the long-range interaction.

randomly from the list. The improvement in the acceptance ratio is clear in the whole range of Θ_H as shown in Fig. 4.7.

We carried out the MC simulation on 10×10 unit cell with periodic boundary condition. The simulation ran the first 10,000 MC steps to allow system to equilibrate, followed by 50 million MC steps for the measuring process. This process was repeated from a single H loading ($\Theta_H = 0.01$) up-to 100 ($\Theta_H = 1$) loadings to study dependence on H loadings on Pt(111). For our implementation of a pseudo random number generation (PRNG) process on a computer simulation, we used the Mersenne Twister library [87], which is widely known as one of the best PRNGs available today. We have done the simulation using mostly the parameter set for the lattice gas model as shown in Tables 4.5 and 4.6.

We have also done the simulation using different parameter set that includes long-range interactions (Table 4.7) for comparison. The interaction range was found to affect the g-value at low temperature region (58K) as might be expected, but at room temperature (273K), the resulting g-value is not so sensitive to the range (Fig. 4.8).

4.3.3 Results of MC simulations

The results of the MC simulation performed at 303 K is shown in Fig. 4.9. Here we have used the long-range interaction parameters. We found that the g-values, g and $\bar{g}$ (the upper panel), are almost the same in the range ($0.15 \leq \Theta_{\mathrm{H}}$). Outside that range, however, we could not obtain reliable ΔS, presumably due to insufficient sampling with the Kawasaki-type MC simulation. So, we will compare with experiment within $0.15 \leq \Theta_{\mathrm{H}}$, neglecting thereby the difference between g and $\bar{g}$; so our comparison is equivalent to comparing the differentiated enthalpy obtained theoretically and that obtained experimentally. The calculated g-value increases from zero as the coverage is increased from zero, and then saturates as the coverage exceeds 20 %. When the coverage exceeds 80 % it decreases towards zero and the g-value curve is approximately symmetric at 50 %, indicating a kind of particle-hole symmetry such that the system can be characterized near 1 ML in terms of the vacant site. The g-value is $g = 11.6$ at the peak and is $g = 10.5 \pm 1$ when averaged in the range $0.2 \lesssim \Theta_H \lesssim 0.8$. The average is smaller than $g = 12$ measured by Marković *et al.* [11] in $HClO_4$ and $g = 11$ by Zolfaghari and Jerkiewicz [9] in H_2SO_4, and $g = 12.2 \pm 1.5$ by Lasia [14] in $HClO_4$ (Fig. 4.9). The experimental curve of Lasia gradually increases at around 0.3 ML but our theoretical curve shows a mild peak at 0.6 ML.

To see the reason for the underestimation, we performed a simulation restricting to the fcc or to the top. When restricting to the fcc we obtained $g = 11 \pm 0.5$, and when restricting to the top, $g = 16.5 \pm 0.8$ (Fig. 4.9). The change in the g-value is quite small when restricted to the fcc only, which indicates dominated H on the fcc. The larger g-value obtained by restricting to the top only can be explained by stronger repulsive interaction for H on the top.

To further investigate the property of the lattice gas model, we performed MC simulations by changing the parameters. First, we changed $\varepsilon_{\mathrm{top}}$ relative to $\varepsilon_{\mathrm{fcc}}$ (Fig. 4.10). When $\varepsilon_{\mathrm{top}}$ was shifted up, the g-value curve did not change reflecting the dominance of $\mathrm{H_{fcc}}$. When it was shifted down, the g-value was increased at lower coverage region ($\Theta_{\mathrm{H}} \lesssim 20\%$), while the increase was not significant at the larger coverage region. We could not find a clear reason for the different effect on g for different Θ_{H}, but we consider that, as $\mathrm{H_{top}}$ is increased in number, there will be complex competition between (1) increase in the interaction because of stronger $\mathrm{H_{top}}$-$\mathrm{H_{top}}$ repulsion and (2) reduced interaction because of availability of both sites. These results show that the experimental results can be explained by taking the $\varepsilon_{\mathrm{top}}$ as optimized by the DFT calculations or by taking larger values.

Then we analyze the number of $\mathrm{H_{top}}$ and $\mathrm{H_{fcc}}$ (Fig. 4.11). We find that the dominance of $\mathrm{H_{fcc}}$ becomes clear only for $\Theta_{\mathrm{H}} > 0.1$ when using the original parameter set, while the dominance is clear in the whole range of Θ_{H} when $\varepsilon_{\mathrm{top}}$ is shifted up only by 17 meV. When shifting down $\varepsilon_{\mathrm{top}}$ by 69 meV, $\mathrm{H_{top}}$ is dominant only for $\Theta_{\mathrm{H}} < 0.3$. These results indicate that $\varepsilon_{\mathrm{top}}$ affects quite sensitively on the dominant sites.

We then study the effect of the interaction energy. When, the interaction energy was scaled up by 10 % in the simulation with the fcc only, the g-value was found enhanced by about 20 %. The g-value curve is then much closer to the experimental one (Fig. 4.12). Therefore, we can conclude that our DFT calculation provides parameters that underestimate the H-H repulsion by 10 %.

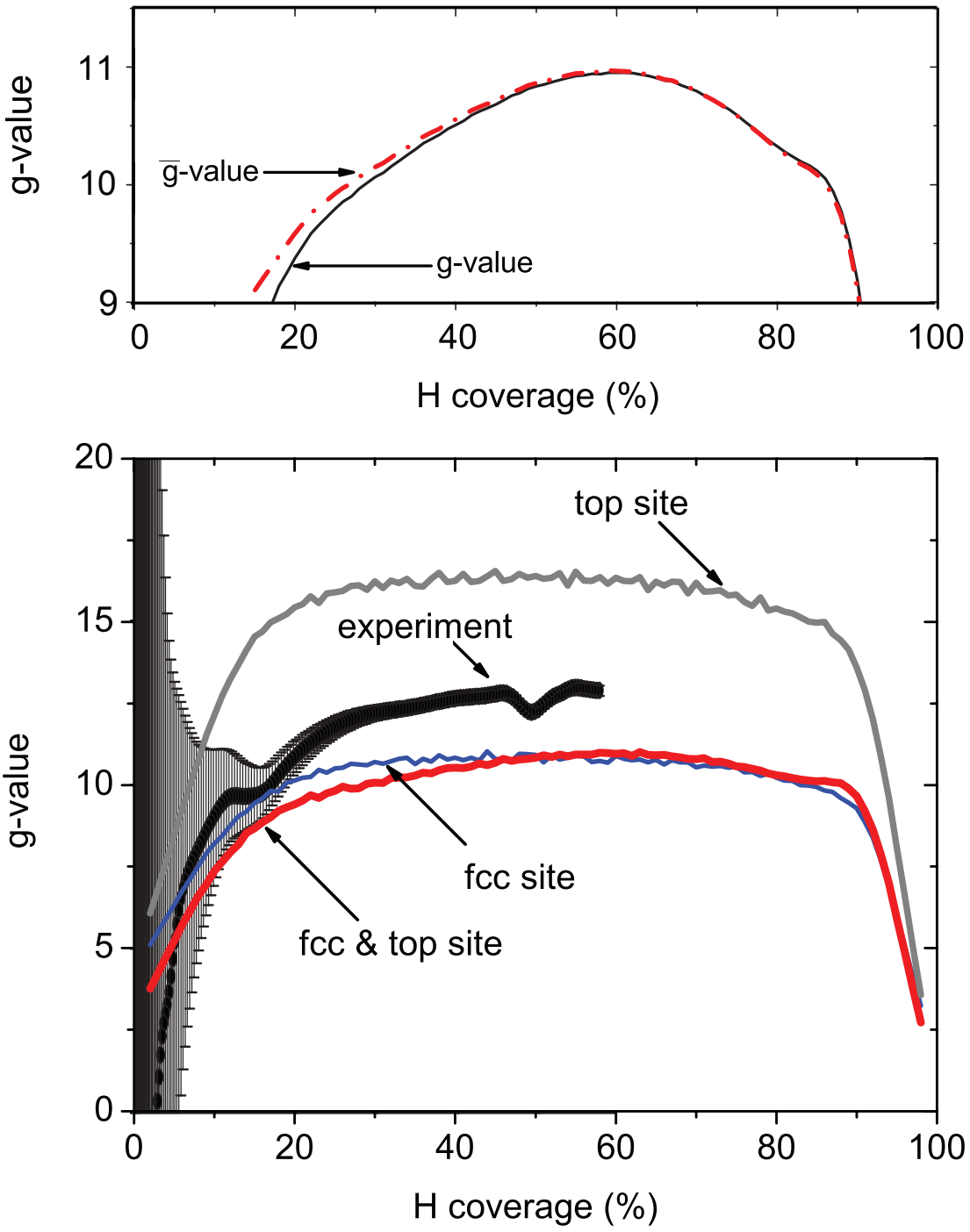

Figure 4.9: The calculated H-H interaction parameters. In the upper panel plotted are g and $\bar{g}$, and in the lower panel compared are the g-values obtained from simulations (solid lines) and from an experiment (Ref.[14]). The experimental data are shown with error bar. The read line corresponds to the simulation using both fcc and top sites, and the blue (gray) line to the simulation with fcc (top) sites only.

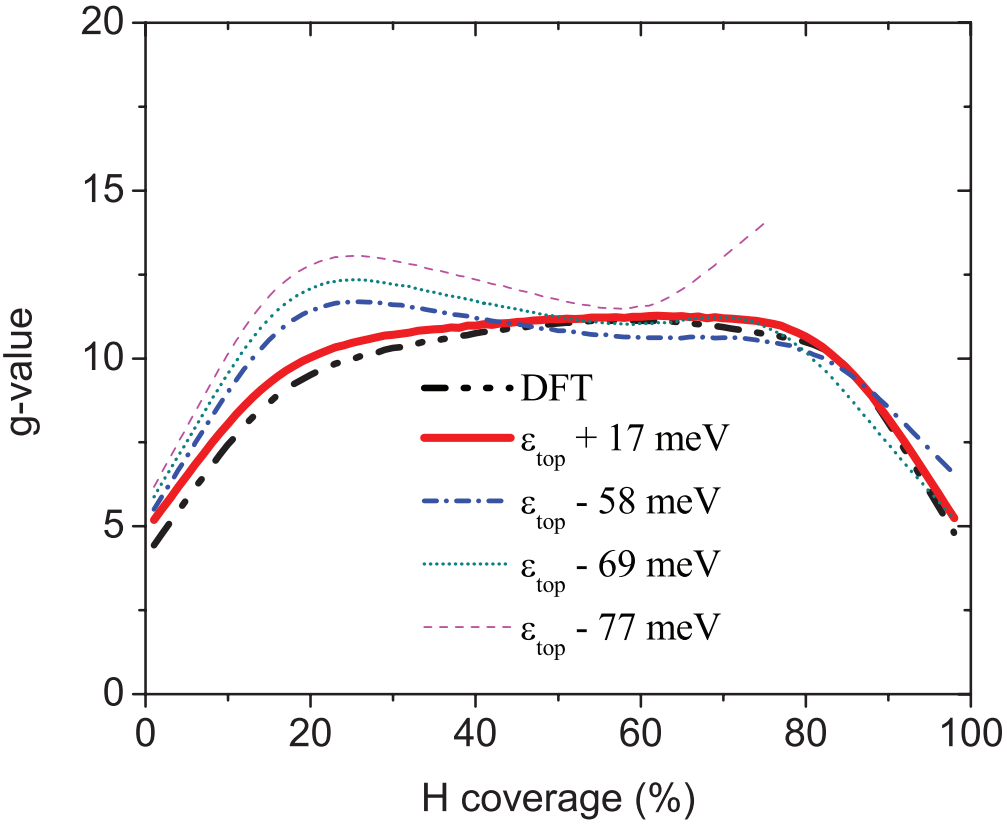

Figure 4.10: g-value curves obtained by shifting the on-site energy of the top relative to the fcc. "DFT" corresponds to the original set of parameters determined by the DFT calculation.

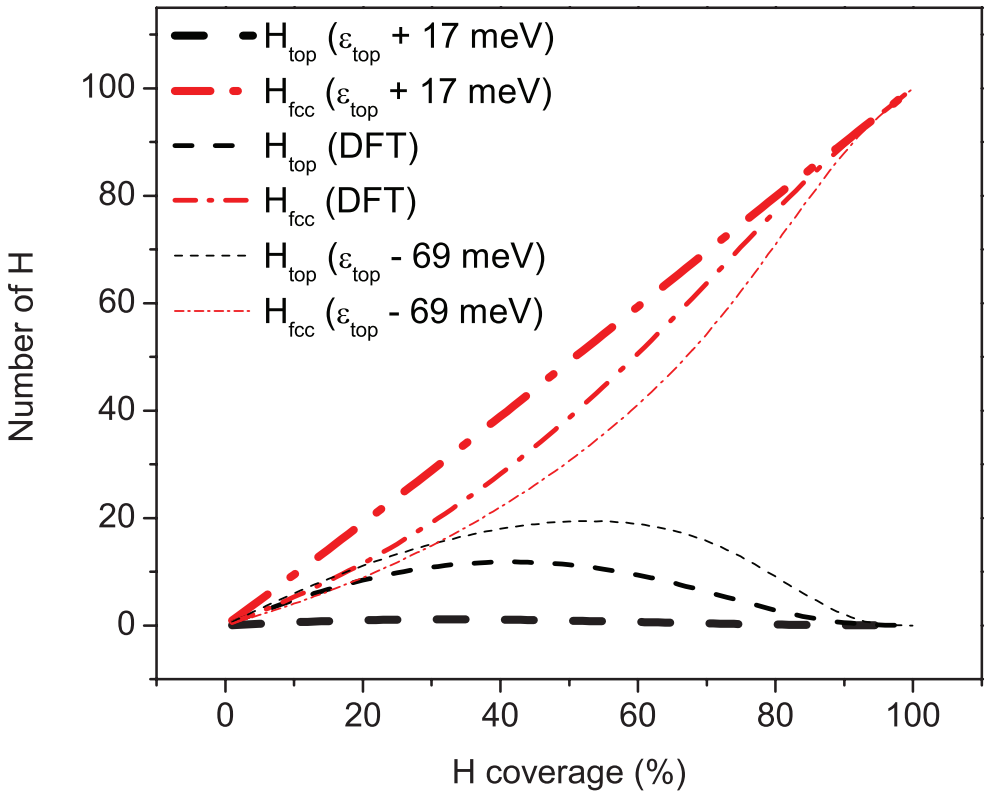

Figure 4.11: The population of H on the top and that on the fcc. The calculation was done by shifting the on-site energy of the top relative to the fcc. "DFT" corresponds to the original set of parameters determined by the DFT calculations.

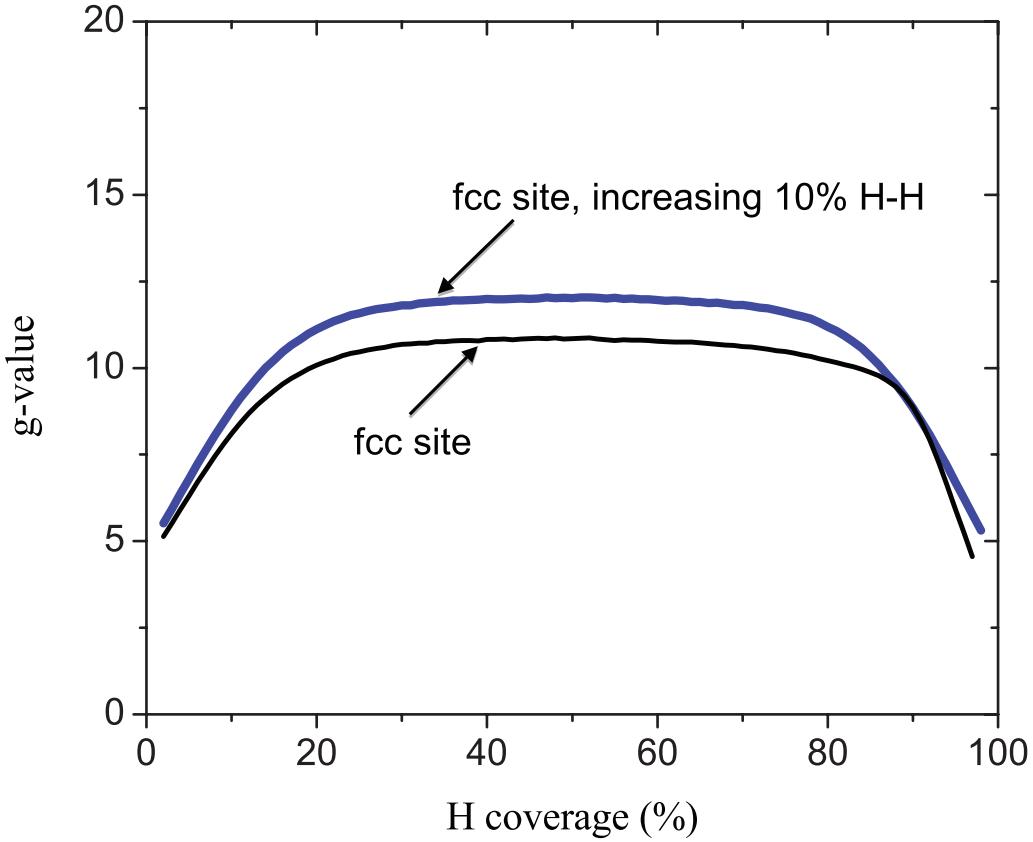

Figure 4.12: g-value curve obtained by enlarging the H-H interaction energy. The simulation was done using the fcc only.

4.3.4 Discussion on voltage dependence of the Pt-H stretching frequency

Finally, we study how the vibrational frequency of Pt-H_{top} stretching motion is affected by nearby H atoms to discuss the effect of electrode potential. When H_{top} is isolated, the Pt-H stretching frequency is 2167 cm^{-1} while when surrounded by three nearest H_{fcc}, the frequency is reduced by 81 cm^{-1}. From our MC simulation, average number of nearest H_{fcc} increase with Θ_H by the rate 0.97/ML. The experimental data of Marković [7] shows that Θ_H increases with the rate 0.43 V/ML and thus 2.25/V for the rate of change in the number of nearest H_{fcc}. Therefore, the rate of change in the stretching frequency is -184 cm^{-1}/V. It is interesting that the rate is not so different from the rate found for the polycrystalline Pt surface -130 cm^{-1}/V [75] despite difference in the surface geometry. It will be then an important target of a future work to investigate if this is just a coincidence or not.

4.4 Conclusion

The hydrogen adsorption on the Pt(111) surface was investigated using a converged first-principles DFT-GGA calculation and a Monte Carlo simulation. It was shown that H_{fcc} is more abundant than H_{top} in consistent with the CV experiment in the literature. Further precise comparison with experiment shows that the H-H interaction is underestimated by 10 %. Possible origin of the discrepancy is the hydration effect neglected in our model although we cannot exclude the possibility that error of the DFT-PBE will also play a role.

Chapter 5

The missing row Pt(110)-(1×2)

5.1 Introduction

Within the past 3 decades, electrochemical surface science has become an important tool in a number of diverse fields such as microelectronics, catalysis, and fuel cells [7, 70]. Among others, the hydrogen-platinum system is one of the most intensively investigated model systems [8, 26, 14, 11, 74, 75, 88]. Although (111) surface is the most stable for FCC metals, other surfaces should also be studies because, in practical applications, the catalysts are typically dispersed in small particles embedded in a matrix. It has been shown that, for particles of FCC metals, the most common facets are the low energy (111) and (100) facets [89]. The previous studies suggested that the catalytically active sites are steps on these facets [90] or edges between the facets [91]. In this context theoretical calculations were done by Gudmundsdóttir et al. and Skúlason et al. to investigate the effect of facet. They made use of the fact that the missing row reconstructed Pt(110)-(1×2) surface can be used as a periodic model of edge sites between (111) facets [92, 93]. Subsequently, the interaction of hydrogen with the Pt(110) surface has been studied extensively both experimentally and theoretically [26, 27, 31, 94, 95].

Engstrom *et al.* [26] and Shern [95] carried out low-energy electron diffraction (LEED), temperature-programmed desorption (TPD) and the mirror electron microscope LEED – that can measure the work function change – to study the adsorption of H on the missing-row Pt(110)-(1×2). They supported the usual assumption [26, 39, 96] of highly coordinated H sitting in the deep troughs of the missing rows. Stenzel *et al.* [97] also supported the result using the vibrational spectroscopy meareuement. However, Kirsten *et al.* [98] gave another proposal of a highly coordinated subsurface site on the basis of a direct structure-probing experiment (Helium atom scattering, HAS). On the contrary, Zhang *et al.* [31] performed LEED experiments and DFT calculations to provide an evidence that β_2-H is chemisorbed at the low coordinated short bridge site on top of the outermost Pt rows. Subsequently, Minca et al. [27] used TPD, quantitative LEED, and DFT to find a chemisorption site, called β_2-state, on the outermost close-packed rows under the ideal coverage of 0.5 ML. Adsorption sites on the (111) microfacets, called β_1-state, are occupied only at higher coverage. Note that the β_1 and β_2 states had been well described in Refs. [26, 94, 99]. Most recently, Gudmundsdóttir *et al.* [30] used

TPD measurements and DFT calculations to confirm that, at low coverages, the strongest binding sites are the low coordination bridge sites at the edge. At higher coverages, on the other hand, H is adsorbed on higher coordination sites either on the micro-facet or in the trough. Those various foregoing researches indicate that there is still controvercy regarding determination of the H chemisorption site. To proceed the study it will be important to investigate the chemisorption site more thoroughly including typical and atypical sites.

The first purpose of the present work is to determine the binding sites and obtain the converged DFT data. We then compute the adsorption isotherm using two different simulation software SIESTA and VASP, and compare their results. We will focus on the comparison of the effective H-H interaction, or the g-value, using a Monte Carlo simulation on a lattice gas model parameterized by the results of the DFT calculations. Our study is the first evaluation of the nature of H-H interactions on the missing-row Pt(110)-(1×2) surface. Note that we investigate the H adsorption on Pt(110)-(1×2) up to 1 ML coverage, and the result showed the most stable sites are the short bridge site on top of outermost Pt rows (R), and the on-top site on the micro facet (F). Therefore, the Monte Carlo simulation was done using both R and F sites, then we compare the derivative of the isotherm, which corresponds to the g-value. This is the second topic of this research. Considering the reasonable accuracy of the first-principles approach in determining the effective H-H interaction on Pt(111), as shown in the previous chapter [88], the interaction parameters obtained for Pt(110)-(1×2) will provide a similar important insight.

5.2 Density Functional Theory (DFT) calculations

5.2.1 Computational methods

The DFT approach successfully used in the study of H on pt(111) was similarly applied in this study. We used the linear combination of atomic orbitals (LCAO) and pseudopotential scheme implemented in SIESTA (Spanish Initiative for Electronic Simulations with Thousands of Atoms) [54, 55] for the first-principles electronic structure calculations. Then the plane wave and projector augmented wave (PAW) potentials [56, 57] scheme implemented in VASP (Vienna Ab initio Software Package) [58, 59, 60] was used to supplement the SIESTA result. The models and adsorption sites of the DFT calculation used for the calculation are shown in Fig. 5.1. In the DFT calculation, we used the generalized gradient approximation (GGA) to the exchange-correlation functional due to Perdew, Burke, and Ernzerhof (PBE) [61]. The repeated slab model was used to model the surface and the surface slab was separated from its periodic image by 16.6 Å, by which interaction energy with the image can be reduced to 1 meV. The surface irreducible Brillouin zone was sampled on the k-point mesh generated by the Monkhorst-Pack (MP) scheme [62].

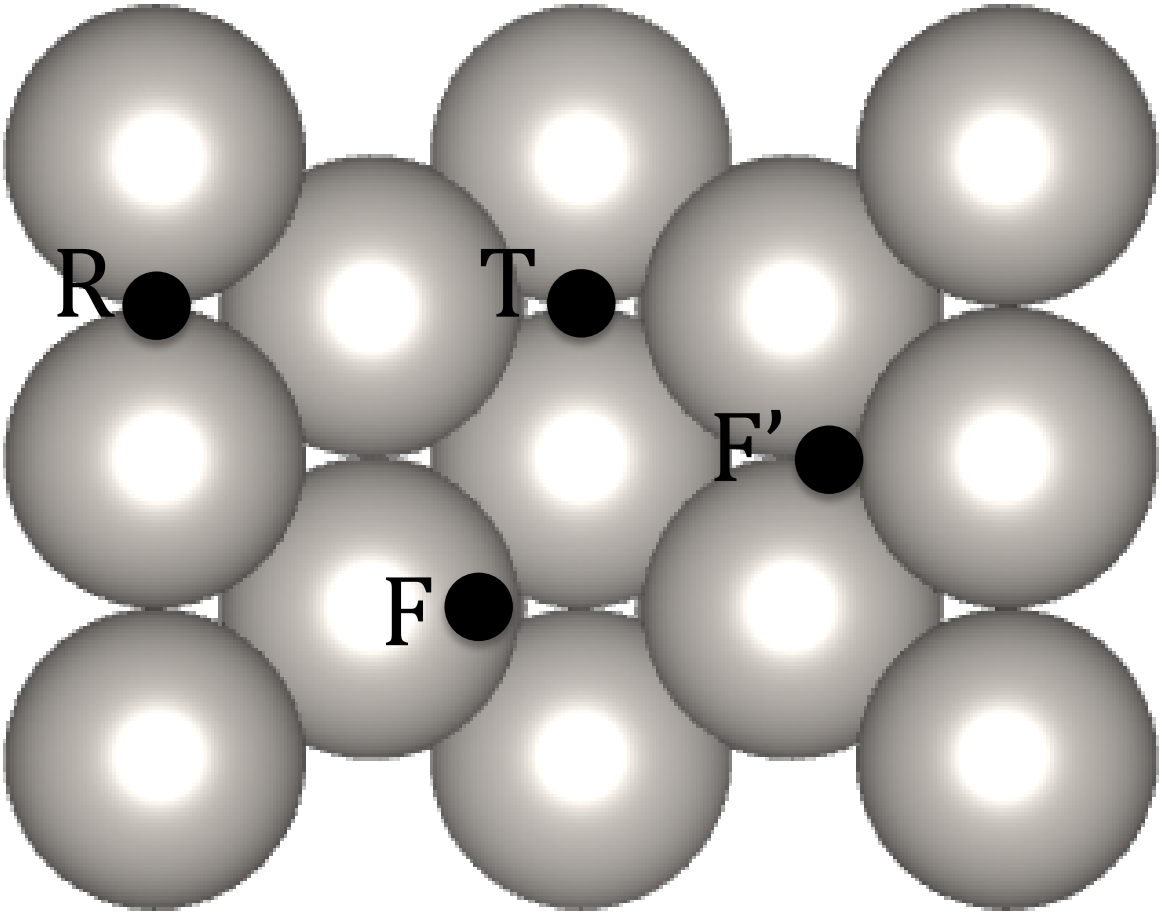

Figure 5.1: The missing row Pt(110)-(1×2) model used for the DFT calculations. The surface was modeled using the repeated slab model. In the DFT calculation, the (1×2) lateral unit cell was used to construct the Pt(110)-(1×2) slabs, on which H atoms were adsorbed on the following sites: the short bridge on the ridge (R), the on-top on the micro facet (F), the HCP hollow site (F') and the long bridge site in the trough (T) such that the coverage ranges from zero to one.

SIESTA calculation

We have adopted the following computational parameters for the SIESTA calculation. We used the double-zeta polarized (DZP) basic set, the mesh-cutoff of 200Ry. We employed the Fermi Dirac function with the electronic temperature of 300 K in carrying out the Brillouin zone integrations. We used the value 200 meV for the energy shift for Pt, which determines the cutoff radius per angular momentum channel. For adsorbed H atoms, more extended basis is used where we used the value 60 meV for the energy shift, and split norm of 0.53 for the second zeta. This ensure to obtain correct bond length and energy of H2 molecule, and is important for the long range interactions [88]. These standard computational parameters used in SIESTA calculation provided reasonably accuracy both in the calculation of a bare Pt surface and a H molecule [88]. The optimized lattice constant of the bare missing row Pt(110)-(1×2) is 3.93 Å in good agreement with the experimental bulk lattice constant (3.924 Å) [78].

The calculation of the H adsorbing surfaces was done for the following three sets of configurations. First, one H atom was adsorbed on the missing row Pt(110)-(1×2) surfaces of (1×2) and (3×2) lateral unit cell. A vacuum equivalent to a twelve-layer slab separated the Pt slabs, where the interlayer spacing was taken as 1.387 Å. The total energy was obtained after relaxing all the H and the Pt atoms of the upper four Pt-layers. This calculation was done mainly for the sake of comparing with previous calculation regarding the stability of binding sites. Second, the surface of (1×2) lateral unit cell was used to investigate convergence property with respect to the number of Pt layers and the k-point mesh. Third, the surface of (3×2) lateral unit cell and nine Pt layers were used to let H atoms adsorb on the short bridge on the ridge (R) and the on-top on the micro facet (F) sites. In the third case, all possible configurations with the H coverage up to 1ML were generated and the calculated total energies were fitted to a lattice gas model as detailed below. We used the spin-polarization calculations for all system. In the Brillouin zone integration, 84 and 12 special k-points were used to sample the (12×12×1) and (4×4×1) MP grids for the (1×2), and (3×2) lateral unit cells, respectively. The zero point energy (ZPE) of H was calculated by displacing the position of H around equilibrium position both in the surface normal and surface parallel directions and by using a harmonic approximation. The ZPE calculation was done using those configurations adsorbed on the same binding sites, *i.e.*, the R-sites or the F-sites, only.

VASP calculation

The VASP calculation was similarly done for three above sets of H-Pt configurations. Besides, we have used the k-point mesh ranging from (7×7×1) to (24×24×1) MP grids for the (1×2) lateral unit cell. We have used the following computational parameters. The plane wave cutoff energy was 400 eV, which is large enough to converge the total energy within the order of 1 meV per atom. Brillouin zone integrations were carried out by employing the Gaussian smearing function with width 0.02 eV. The optimized lattice constant of the bare missing row Pt(110)-(1×2) obtained from VASP calculation is 3.92 Å. The ZPE calculation was not calculated in VASP calculation.

cell	Pt layers	R	F	F′	T
			1/3 ML		
(1×2)	5	−0.649	−0.605	−0.564	−0.545
	7	−0.666	−0.632	−0.507	−0.497
	9	−0.737	−0.621	−0.497	−0.445
		(−0.555)	(−0.428)	(−0.343)	(−0.270)
			1/9 ML		
(3×2)	9	−0.710	−0.675		
		(−0.526)	(−0.452)		

Table 5.1: The adsorption energy of H (eV). The results from VASP calculation are parenthesized.

5.2.2 DFT-GGA description of H on missing row Pt(110)-(1×2)

Adsorption sites

Previous calculations showed that the energy associated with the various binding sites on the surface is strongly dependent on the H-atom coverage. By adding the H-atoms to the surface one at a time, the surface is filled first at the strongest binding sites and finally at the weakest ones [30]. In this context, we firstly test the order of adsorption sites, they get filled by calculating the hydrogen adsorption energy

$$E_{\text{ads}} = E_{\text{tot}}(N_{\text{H}}) - E_{\text{tot}}(0) - \frac{n_{\text{H}}}{2} E_{\text{H}_2},$$

where $E_{\text{tot}}(N_{\text{H}})$ is the total energy of the Pt surface adsorbed with N_{H} H atoms and E_{H_2} is the total energy of the isolated H molecule. E_{ads} shows that the short bridge site on the ridge (R) is the strongest adsorption site, then the on-top on the micro facet (F), and finally the HCP hollow site (F') and the long bridge site in the trough (T) (see Table 5.1). This result is in agreement with the results of Zhang et al. [31] and Gudmundsdóttir et al. [30]. Besides, Gudmundsdóttir et al. has shown that when the ridge has been filled, the preferred sites are the tilted on-top sites on the micro facets (F) followed by adsorption onto the long bridge sites in the trough (T). The filling of the trough sites forces the neighboring H-atoms to move from the on-top sites towards the HCP threefold hollow sites on the (111) micro facet (F').

Secondly, we calculate the optimized Pt-H bond lengths for the H on the Pt(110)-(1×2) as shown in Table 5.2. We have confirmed that the results were affected by less than 1% when changing the number of Pt layers from five to nine. The averaged ZPE of H on the R and the F were calculated using only the (3×2) lateral cell. The results are 160 meV and 184 meV, respectively, for the R and the F sites. To obtain the converged value, we now investigate in detail the convergence property with respect to the number of Pt layers and k-points.

Previous calculation for Pt(111) provided the dependence of the adsorption energy on k-point mesh and number of Pt layers [88]. Therefore, in this work, the calculation was done similarly using (1×2) lateral unit cell, on which one H atom was let adsorb either on the R or on the F. Table 5.3 shows the calculated adsorption

cell	Pt layers	R	F	F′	T
		1/3 ML			
(1×2)	5	3.9	2.9	3.0	2.5
		(3.8)	(3.0)		
	7	3.9	2.9	2.9	2.4
		(3.8)	(3.0)		
	9	3.9	2.9	2.8	2.4
		(3.8)	(2.9)	(2.8)	(2.6)
		1/9 ML			
(3×2)	9	3.8	2.9		
		(3.7)	(3.0)		

Table 5.2: The optimized Pt-H bond length (Å). The results from VASP calculation are parenthesized.

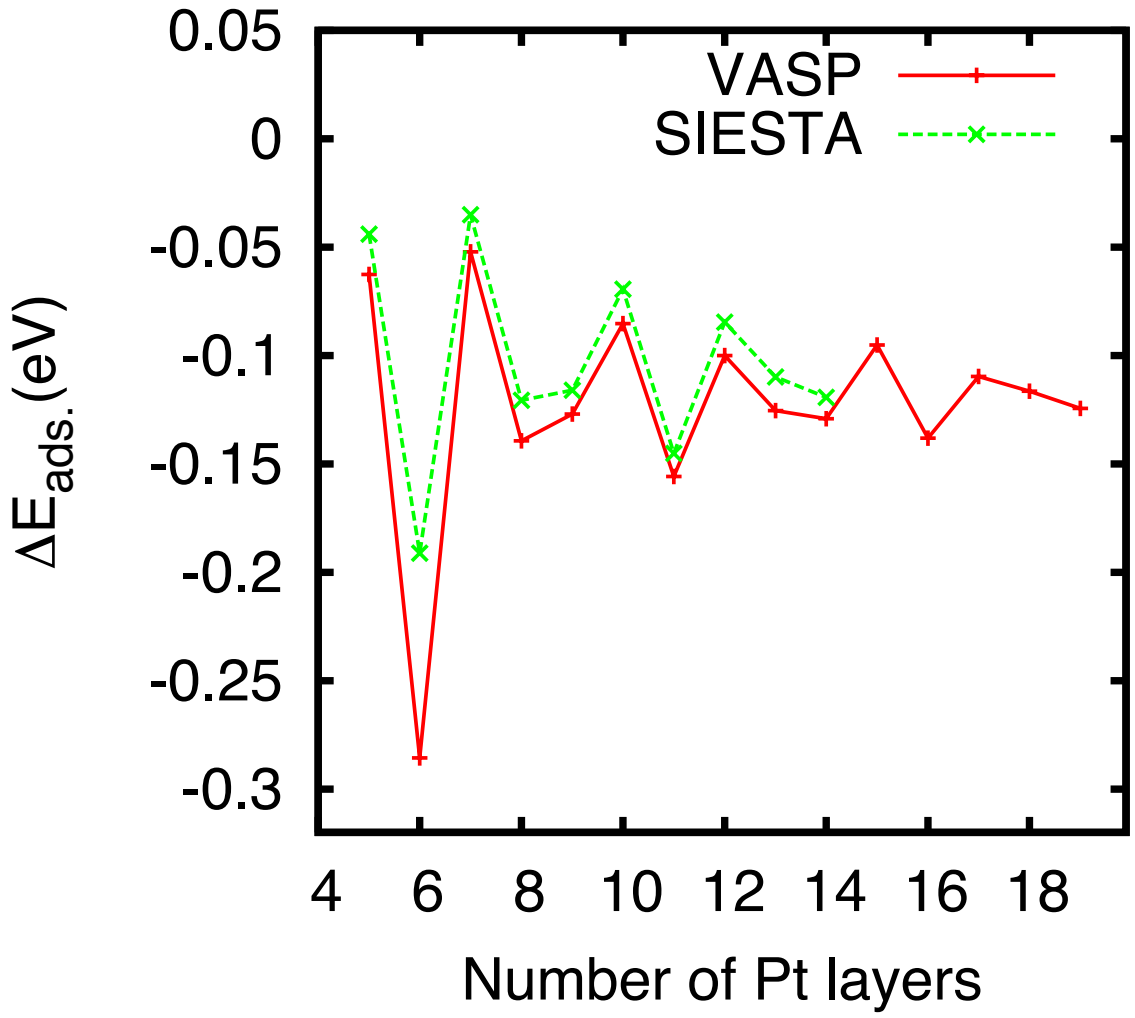

Figure 5.2: The relative adsorption energy, $E_{\mathrm{ads}}(\mathrm{R}) - E_{\mathrm{ads}}(\mathrm{F})$, calculated using SIESTA and VASP.

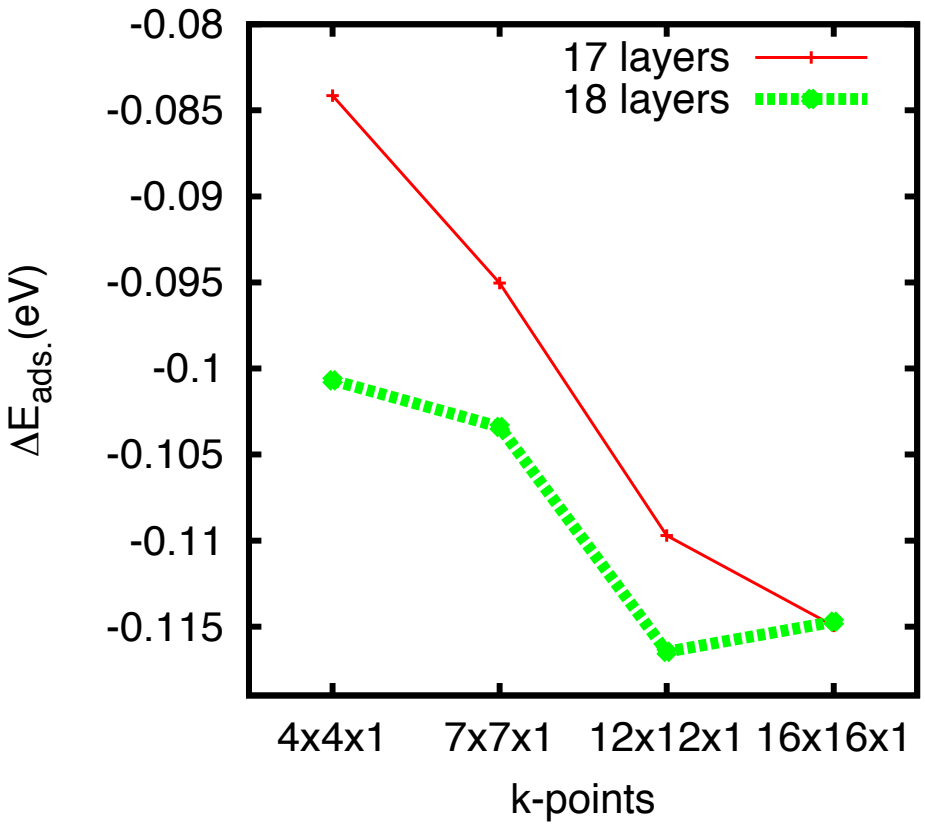

Figure 5.3: k-point dependence of ΔE_{ads}.

Pt layers	SIESTA		VASP	
	R	F	R	F
5	-0.649	-0.605	-0.483	-0.420
6	-0.770	-0.579	-0.597	-0.311
7	-0.666	-0.631	-0.492	-0.440
8	-0.715	-0.594	-0.537	-0.398
9	-0.737	-0.621	-0.555	-0.428
10	-0.683	-0.614	-0.507	-0.422
11	-0.743	-0.598	-0.562	-0.407
12	-0.703	-0.619	-0.523	-0.423
13	-0.718	-0.608	-0.542	-0.417
14	-0.735	-0.615	-0.551	-0.422
15			-0.521	-0.426
16			-0.553	-0.415
17			-0.534	-0.425
18			-0.535	-0.418
19			-0.550	-0.425

Table 5.3: The adsorption energy of H (eV), using (12×12×1) MP grid for SIESTA and VASP calculations.

energy and Fig.5.2 plots the adsorption energy on the F relative to that on the R, $\Delta E_{\rm ads}$. The table shows that the SIESTA calculation provides the adsorption energy systematically larger by 0.15 eV in magnitude, while the figure shows that they provide a similar dependence on the number of Pt layers as it changes from 5 to 19 layers when (12×12×1) MP grid was used. From the Fig. 5.2 we found that for the low Pt layers (less than 9), the value oscillates with large amplitude, then the oscillation is regular and periodic when taking 9 to 19 layers. It suggests that the converged value has already been determined well around -0.12 eV within the amplitude of the oscillation ($\sim$ 40 meV) by taking these layers. Fig. 5.3 plots the dependence on k-points, which shows that the results for various number of Pt layers becomes very close to each other when using (16×16×1) MP grid. From these results we conclude that the converged $\Delta E_{\rm ads}$ is located at around -0.12 eV. When adding ZPE, the value becomes -0.14 eV, or the R obviously is more stable by that amount. This is our conclusion on the theoretical adsorption energy within the UHV surface and DFT-PBE. We will show below the effective H-H interaction parameters that have not been investigated before in theoretical and experiment. In doing the investigation thermodynamically, we use the nine layer slab system, which is showed that the converged value of $E_{\rm ads}$ obtained ~ -0.12 eV (see Table 5.1).

Mapping to a lattice gas model

Now we show and compare the geometry parameter changes during the structural search. 45 configurations of the H-adsorptions on the missing row Pt(110) on the (3×2) lateral unit cell have been simulated for all hydrogen positions on R and F sites. Our calculation shows that the geometry parameters agree very well between

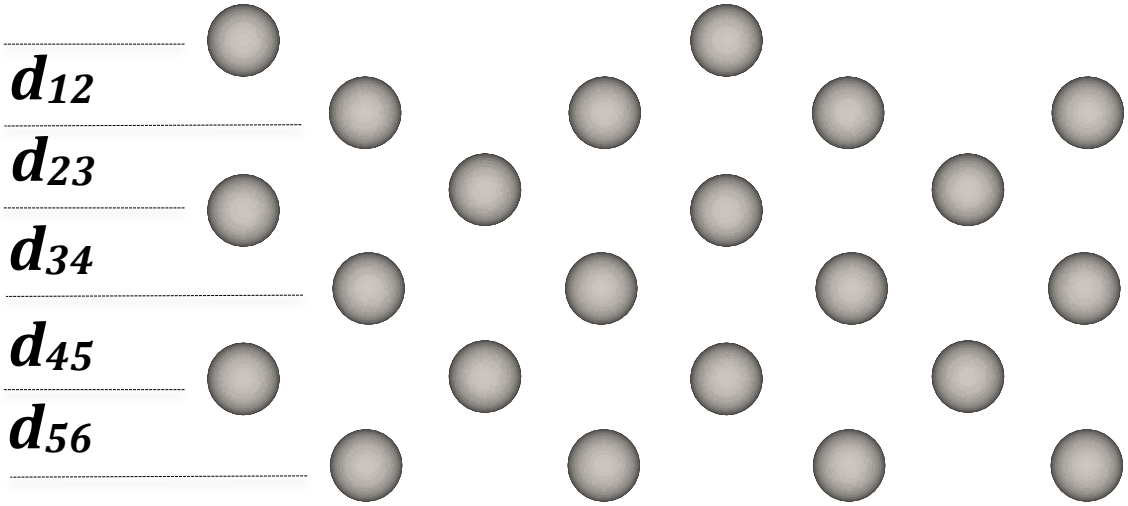

Figure 5.4: Side view of the missing-row reconstructed H/Pt(110) surface. $d_{i,(i+1)}$ denotes the (average) inter-layer spacing in layer i.

System	LEED	LEED	DFT			SIESTA				VASP	
method	clean	β_2-H	Full R	β_2-H	Full R	β_1-H	Full 1ML	β_2-H	Full R	β_1-H	Full 1ML
config.	[100]	[31]	[31]								
d_{12}	1.15	1.25	1.32	1.25	1.36	1.34	1.28	1.24	1.36	1.34	1.24
d_{23}	1.37	1.36	1.33	1.42	1.39	1.41	1.47	1.40	1.37	1.39	1.48
d_{34}	1.41	1.41	1.43	1.43	1.45	1.45	1.42	1.44	1.46	1.45	1.46
d_{45}	1.40	1.38	1.42	1.45	1.44	1.44	1.45	1.45	1.44	1.45	1.46
d_{56}	1.38	1.39	1.36	1.42	1.42	1.42	1.42	1.42	1.42	1.42	1.42

Table 5.4: Experimental and theoretical parameters for the missing-row structure of the clean inter-layer spacing and hydrogen-modified H/Pt(110)-(1×2) surface. $d_{i,(i+1)}$ denotes the (average) inter-layer spacing in layer i (all values in Å). Error limits for the parameters derived by the LEED analysis from Zhang et al. [31] are ±0.02 Åfor $\Delta\, d_{i,(i+1)}$. For DFT calculation: full R: all R sites filled, full 1ML: all R and F sites filled.

SIESTA and VASP method, and they are also in fair agreement with previous experimental and theoretical calculation[31, 100] (see Table 5.4 and Fig. 5.4). The most important change upon hydrogen adsorption is the relaxation in the first interlayer spacing d_{12}. The change amounts to 0.10 Å, well exceeding the combined error limits of both experiments and DFT for hydrogen-modified β_2-H/Pt(110)-(1×2) surface. The other interlayer spacings and the buckling in the third layer stay roughly the same within experimental errors. Zhang et al. has stressed that the substantial change of relaxation ~ 0.1 Å observed here is much less than the corrugation change (0.5 Å observed in the HAS experiment by Kirsten et al. [98]). This difference in corrugation and relaxation measured in the HAS and LEED experiments, respectively, is precisely the experimental information pinpointing the adsorption site of the β_2-hydrogen on Pt(110) [31].

We then fit the adsorption energy results to a lattice gas model by the form,

$$H = \sum_{\alpha} \varepsilon_{\alpha} n_{\alpha} + \sum_{\alpha\beta} v_{\alpha\beta} n_{\alpha} n_{\beta},$$

site	SIESTA	VASP
R	$-0.699(-0.543)$	-0.523
F	$-0.674(-0.493)$	-0.444

Table 5.5: The fitted on-site energy (eV). The data corrected with ZPE is shown in parenthesis.

H-H pair	energy		
H_R-H_R	-0.038 (-0.032)		
H_R-H_F	0.073 (0.073)		
H_F-H_F	0.055 (0.057)	0.039 (0.042)	0.022 (0.025)

Table 5.6: The fitted interaction energy (eV) obtained from SIESTA calculation. The data corrected with ZPE is parenthesized.

where ε_α is the on-site energy for $\alpha \in \{\text{R and F}\}$ and $v_{\alpha\beta}$ is the pair-wise interaction energy. Those pairs with distance less than 2.26 Å were omitted by assigning infinite energy, and among those with larger distance, the smallest one were assigned finite value. Under these constraints, the total energies of SIESTA and VASP were fitted using the standard regression algorithm. Resulting values are listed in Tables 5.5, 5.6 and 5.7. The mean errors of the fitting are $\sim$15 meV, $\sim$10 meV and the maximum errors are $\sim$41 meV, $\sim$27 meV for SIESTA and VASP, respectively.

The zero point energy (ZPE) was fitted independently for SIESTA calculation as follows. ZPE was calculated by diagonalizing the dynamical matrix as stated above for all the configurations adsorbed at the R sites or the F sites only; the results were subsequently averaged over the configurations of the same coverage to get $E_{ZPE}(\Theta_H)$. The coverage dependence of ZPE is shown in Table 5.8. The averaged ZPE energy was then used to correct the on-site and interaction energies (Tables 5.5 and 5.6).

From the H-H interaction result, it is interesting to note that a strong attraction can be seen between the H-adatoms on the ridge, while there is a weak repulsion on the micro facets when VASP is applied (Table 5.7). This is in good agreement with the recent theoretical study [30]. However, SIESTA result shows that the value of the H_R-H_R attraction and the H_F-H_F repulsion are similar. It may be explained by the change of the corrugation amplitude (ΔZ) (see [30] for the definition of the corrugation amplitude) when using different DFT simulation methods. VASP calculation shows that ΔZ_R and ΔZ_F are 3.71 Å and 2.96 Å, respectively. While

H-H pair	energy		
H_R-H_R	-0.036 (-0.030)		
H_R-H_F	0.041 (0.047)	0.006 (0.000)	
H_F-H_F	0.029 (0.026)	0.017 (0.019)	0.007 (0.011)

Table 5.7: The long-range interaction parameters (eV) for the lattice gas model, obtained from VASP calculation. The values in parenthesis are the original (short-range) parameters.

Number of H	R	F
1	0.158	0.181
2	0.158	0.182
3	0.162	0.184
4		0.185
5		0.186
6		0.188

Table 5.8: The Zero Point Energy (eV) of one hydrogen on the missing-row Pt(110) surface, obtained from SIESTA calculation.

SIESTA result shows that ΔZ_{R} is 3.78 Å and ΔZ_{F} is 2.90 Å. Besides, we observed that the hydrogen on the F-sites has tendency to follow the zigzag line to archive the highest total adsorption energy. This phenomena can be explained based on the lowest value of the $\mathrm{H_F}$-$\mathrm{H_F}$ interaction energy from Tables 5.6 and 5.7. The same order in which H get filled has been showed in previous theoretical calculation [30].

5.3 Monte-Carlo (MC) simulation

5.3.1 Free-energy and effective H-H interaction

Having constructed the lattice gas model, we now perform the MC simulation to compute the free-energy of adsorption, which is used to evaluate the effective H-H interaction $V^{\mathrm{eff}}_{\mathrm{H\text{-}H}}$.

Similar to the previous study [88], we define the effective interaction as the coverage derivative of the adsorption energy. And the Gibbs free-energy were used for the adsorption energy, $G(N_{\mathrm{H}},T)$, subtracted by the configurational entropic term, *i.e.*, to use the enthalpic term $G(N_{\mathrm{H}},T)\ +TS_{\mathrm{config}}(N_{\mathrm{H}},T)$, with the reference free-energy taken to be $G(0,T)+\frac{1}{2}N_{\mathrm{H}}\mu^0_{\mathrm{H_2}}$, where $\mu^0_{\mathrm{H_2}}$ is the chemical potential of hydrogen gas at standard condition. That is, the adsorption energy is

$$E^0_{\mathrm{ads}}(N_{\mathrm{H}},T)\equiv\left[\frac{\partial}{\partial N_{\mathrm{H}}}\left\{G(N_{\mathrm{H}},T)+TS_{\mathrm{config}}(N_{\mathrm{H}},T)-\frac{1}{2}N_{\mathrm{H}}\mu^0_{\mathrm{H_2}}\right\}\right]_T$$

or equivalently

$$E^0_{\mathrm{ads}}(\Theta_{\mathrm{H}},T)\equiv\left[\frac{1}{N_{\mathrm{site}}}\frac{\partial}{\partial\Theta_{\mathrm{H}}}\left\{G(\Theta_{\mathrm{H}},T)+TS_{\mathrm{config}}(\Theta_{\mathrm{H}},T)\right\}\right]_T-\frac{1}{2}\mu^0_{\mathrm{H_2}},$$

where N_{site} is the number of adsorption sites of the system. Then the effective interaction is

$$\begin{aligned}V^{\mathrm{eff}}_{\mathrm{H\text{-}H}}(\Theta_H,T)&=\left(\frac{\partial E^0_{\mathrm{ads}}(\Theta_{\mathrm{H}},T)}{\partial\Theta_H}\right)_T\\&=\left(\frac{1}{N_{\mathrm{site}}}\frac{\partial^2}{\partial\Theta^2_{\mathrm{H}}}\left\{G(\Theta_{\mathrm{H}},T)+TS_{\mathrm{config}}(\Theta_{\mathrm{H}},T)\right\}\right)_T.\end{aligned}$$

We use its dimensionless parameter $V_{\text{H-H}}^{\text{eff}}(\Theta_{\text{H}}, T)/(k_B T)$, which is called as the g-value. This g-value was obtained using the configurational entropy corresponding to a non-interacting system neglecting the effect of the H-H interaction. Effect of the interaction was, however, shown negligible on the Pt(111) surface [88].

5.3.2 MC simulation conditions

The MC simulation was done at a given particle number N_{H} and the temperature T condition. The H site was randomly updated according to the Kawasaki-type dynamics to increase the acceptance ratio. The new site was chosen by the exchange of adsorbed H with a neighboring empty one. The location of H was first listed with its allowed empty sites, or the empty sites that do not interact with other H atoms, and then a H atom was randomly selected from the list.

We carried out the MC simulation on 30×4 unit cell with periodic boundary condition. The simulation ran the first 10,000 MC steps to allow system to equilibrate, followed by 50 million MC steps for the measuring process. This process was repeated from a single H loading ($\Theta_{\text{H}} = 1/120$) up-to 120 ($\Theta_{\text{H}} = 1$) loadings to study dependence on H loadings on missing-row Pt(110)-(1×2). For our implementation of a pseudo random number generation (PRNG) process on a computer simulation, we used the Mersenne Twister library [87], which is widely known as one of the best PRNGs available today.

Firstly, we have done the simulation using the parameter set for the lattice gas model from the SIESTA calculation as shown in Tables 5.5 and 5.6. Then, the second simulation has been done using different parameter set that includes short-range and long-range interactions from VASP calculation (Table 5.7) for comparison.

5.3.3 Results of MC simulations

The results of the MC simulations performed under the temperature 303 K are shown in Figs. 5.5, 5.6, and 5.7; they correspond to the parameter sets determined by the SIESTA calculation and by the VASP calculation, respectively. The results are rather close to each other except for the peak height appearing at $\Theta_{\text{H}} \sim 1/3$ ML. The appearance of this peak can be explained by the appearance of hydrogen on the F site after filling in full H on the R site at 1/3 ML. When the coverage is lower than 1/3 ML, the g-value has large negative value ($\simeq -18$) and increases with the coverage to become close to zero at 1/3 ML. This indicates that the H-H interaction is attractive initially and the attractive force diminishes at 1/3 ML. The behavior at $\Theta_{\text{H}} < 1/3$ ML is consitent with experiment of Lasia (see Fig. 5.7)[14], while not under higher coverage conditions. Lasia obtained the g-value of H/Pt(110) in $HClO_4$ using the cyclic voltammograms (CV). The experimental value is almost zero at $\Theta_{\text{H}} \simeq 1/3$ ML and is reduced to $\simeq -5$ at $\Theta_{\text{H}} \simeq 1$ ML; large fluctuation appears at lower coverages.

The experimental g-value is almost symmetric, $g(1/2 - \Theta_{\text{H}}) \simeq g(\Theta_{\text{H}})$ (see Fig. 5.8), while the theoretical one is not. At $\Theta_{\text{H}} \sim 1/2$ ML $g \simeq 15$ when using the SIESTA parameter set, while it is $\simeq 5$ when using the VASP one, with the latter being closer to the experimental one, $g \simeq 4$. While the theoretical g-value is always positive at

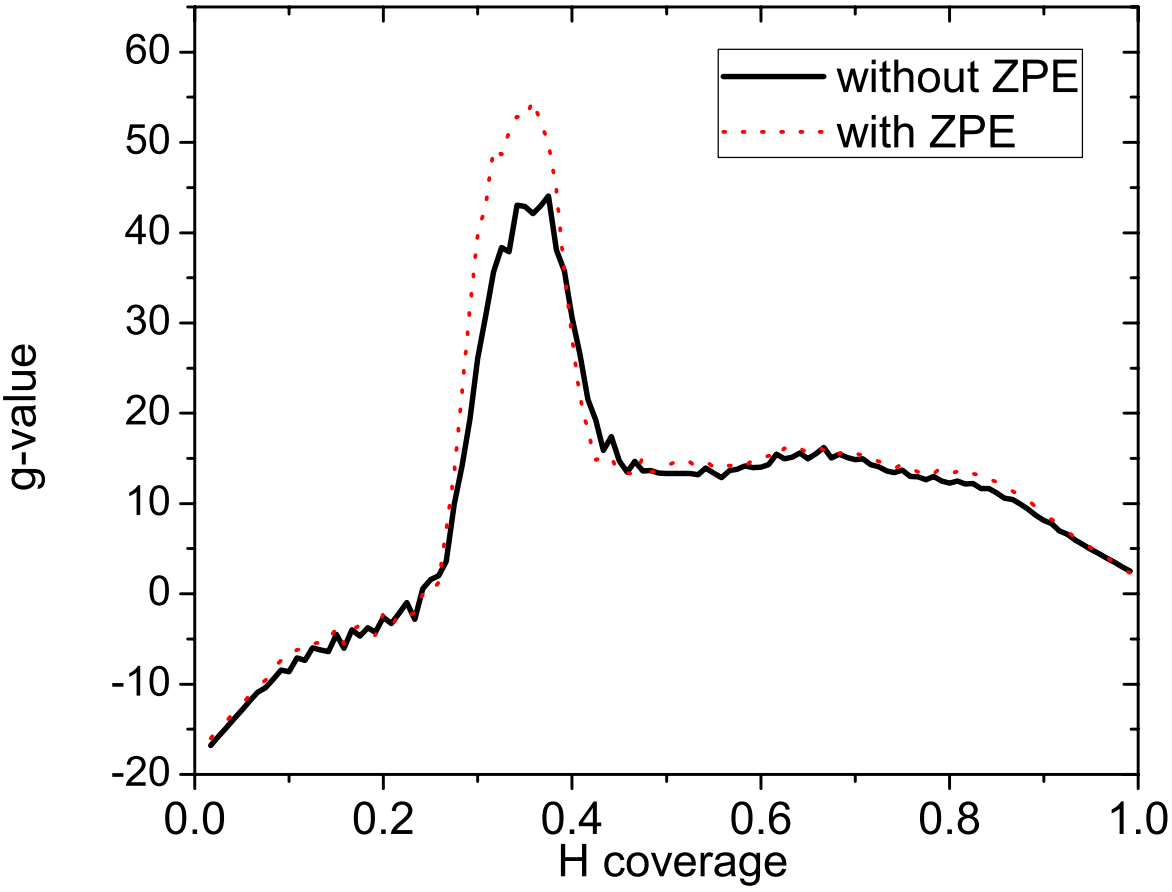

Figure 5.5: The calculated g-value obtained using the SIESTA calculation with and without ZPE correction.

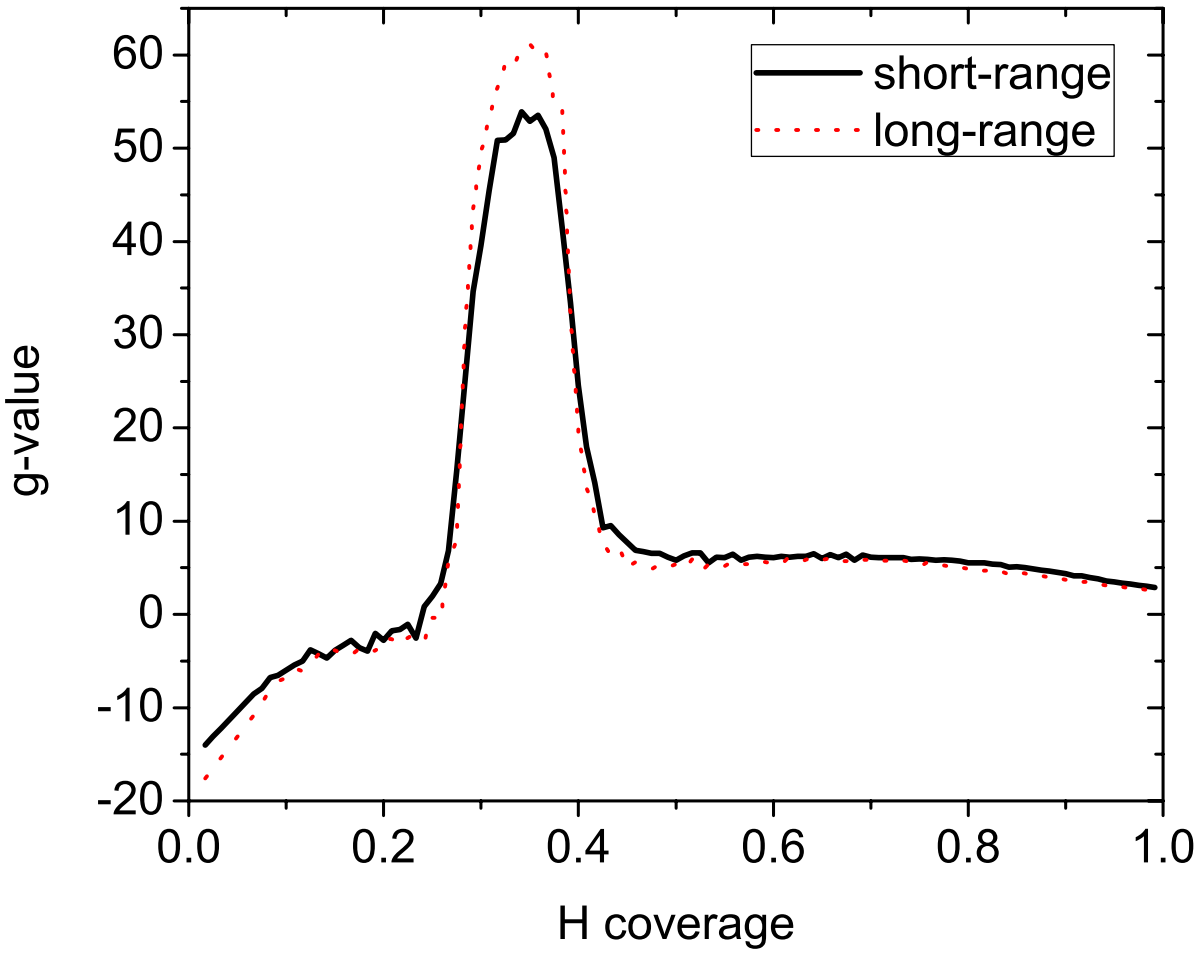

Figure 5.6: The calculated g-value obtained from the VASP calculation using the short-range interaction and the long-range interaction.

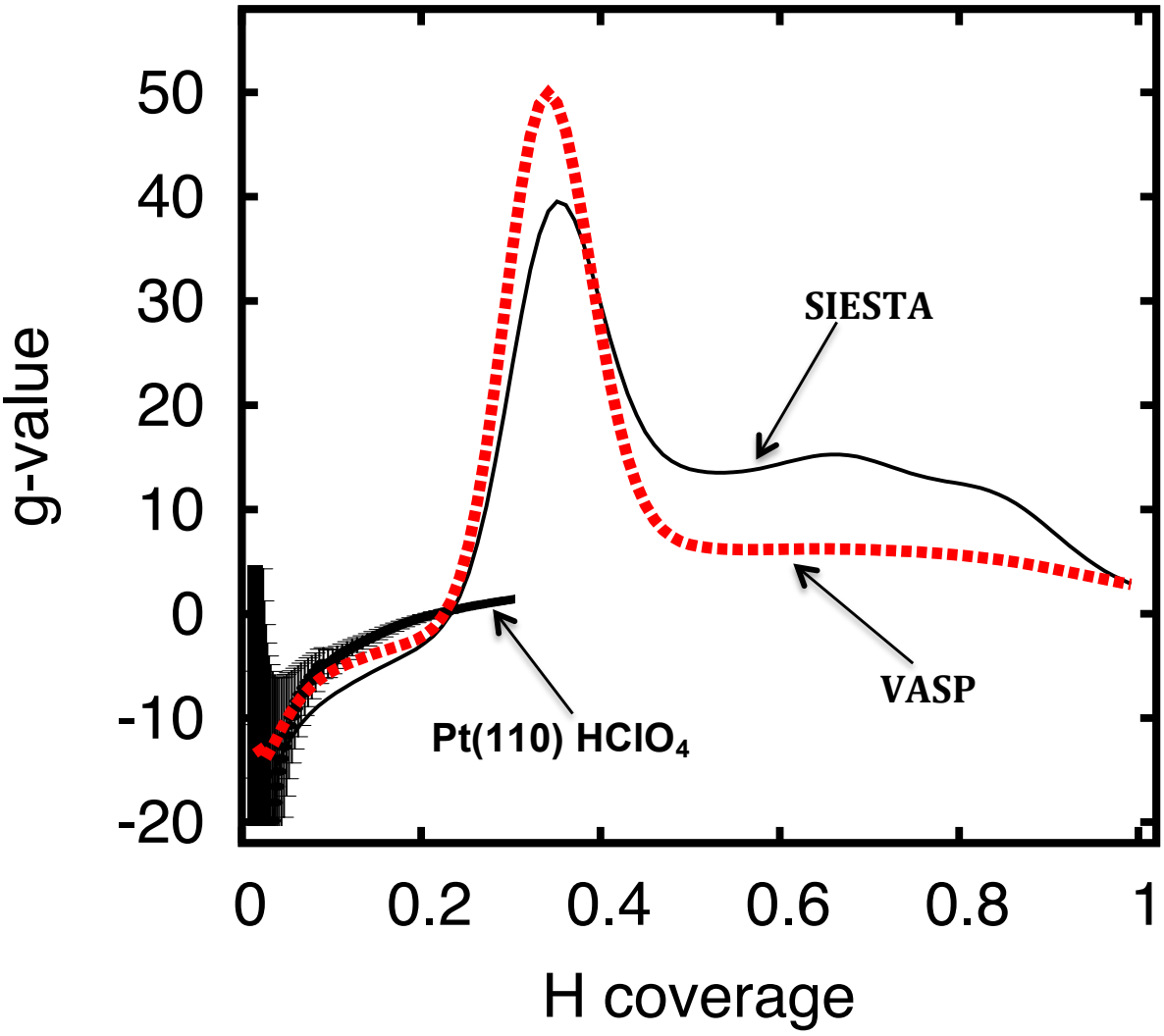

Figure 5.7: The calculated g-value obtained from the VASP and SIESTA calculations, using the Bezier approximation smoothing, and from an experiment [14]. The experimental data are shown with error bar.

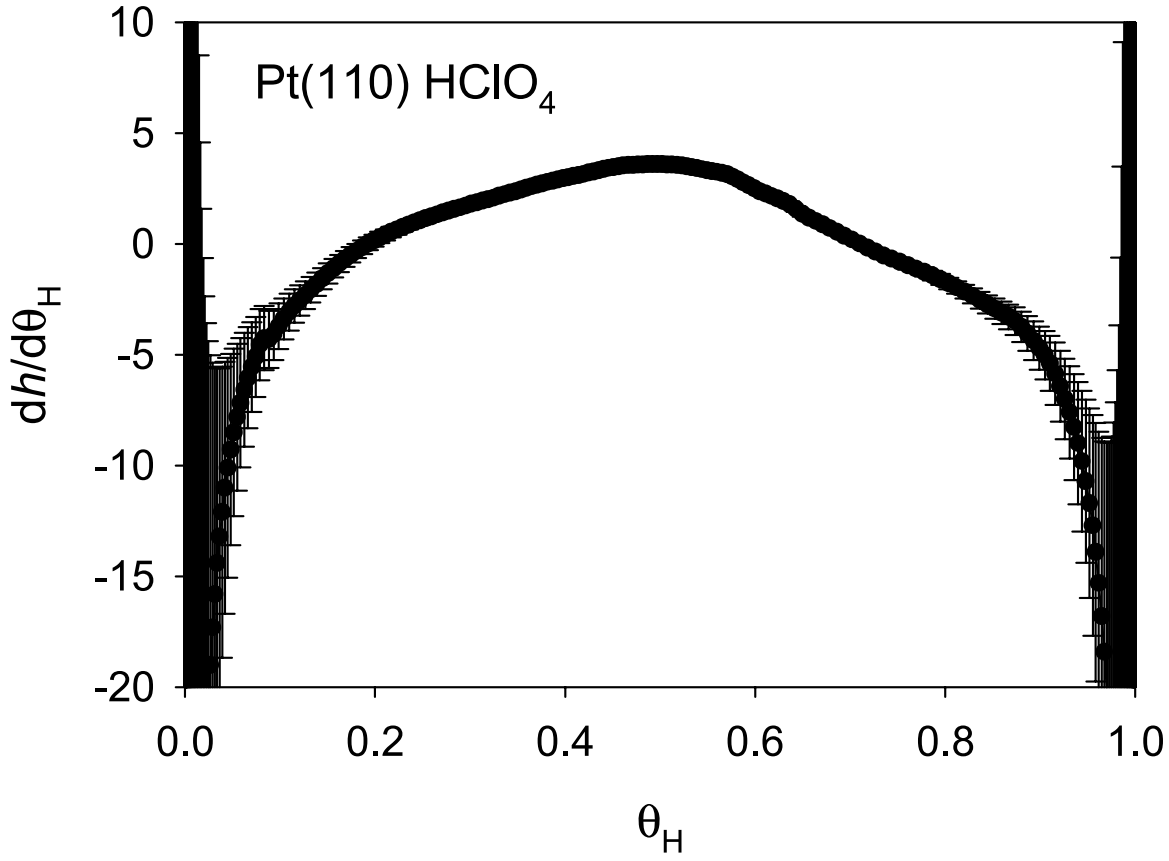

Figure 5.8: The dependence of $dh/d\Theta_H$ on Θ_H on Pt(110) from ref. [14].

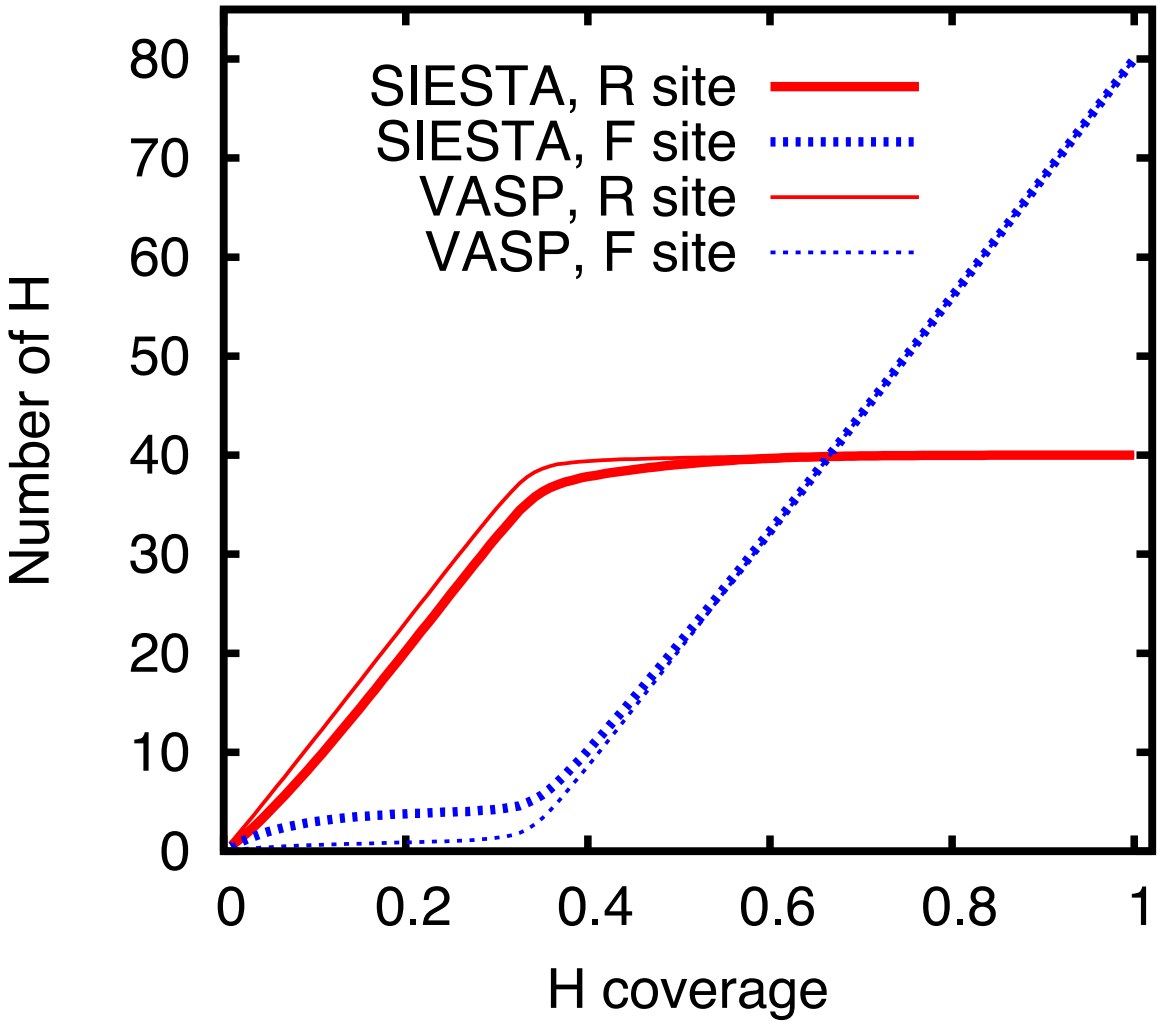

Figure 5.9: The population of H on the R and that on the F sites.

$\Theta_H > 1/2$ ML and diminishes at $\Theta_H < 1$ ML, the experimental one goes negative at $\Theta_H > 0.7$ ML. In this sense, there is qualitative difference in the force between theory (always repulsive) and experiment (attractive near 1 ML).

The peak appearing at $\Theta_H \simeq 1/3$ ML is found to be rather sensitive to the parameter set. The peak height becomes higher by ∼20 % by including the ZPE (Fig. 5.5) and becomes higher by ∼20 % by including the long-range interaction (Fig. 5.6). From the VASP calculation, we found that the g-value is $g = 50$ at the peak and is $g = 6.5 \pm 0.5$ when averaged in the range $0.5 \lesssim \Theta_H \lesssim 0.8$, while it is $g = 40$ at the peak and is $g = 14.5 \pm 0.5$ when averaged in the range $0.5 \lesssim \Theta_H \lesssim 0.8$ in SIESTA result (Fig. 5.7). It means that the g-value of the SIESTA method underestimates the VASP method by 20% at 1/3 ML coverage, and overestimates by two times as coverage exceeds 0.5ML. Possible origin of the discrepancy is from the differently using the potentials scheme implemented in simulated packages. The calculated g-value is in reasonable agreement with experiment [14] in the lower coverage $\Theta_H < 1/3$ conditions and in fair agreement for $\Theta_H > 1/2$, while the theory predicts a distinct peak at $\Theta_H \simeq 1/3$ although no such peak appears experimentally (see Figs. 5.7 and 5.8). Therefore, it seems that there is significant effect neglected in the simulation. The reason for the discrepancy is unfortunately not clear from this study.

Besides, we compared the SIESTA and VASP results using the number of H_R and H_F (Fig. 5.9). We find that the number of H_R otained from SIESTA calcualtion is generally lower than that from VASP calculation although the difference is quite small. The number of H_F in SIESTA result is only slightly higher than in VASP calculation as the coverage is increased from 0 to 0.5 ML, and the two results are very close to each other at higher coverages. These results indicate that the simulation packages only slightly affect on the H sites at low coverage ($\Theta_H \lesssim 0.5$).

5.4 Conclusion

The hydrogen adsorption on the missing-row Pt(110)-(1×2) surface was investigated using a converged first-principles DFT-GGA calculation and a Monte Carlo simulation. It was shown that the H on the bridge on the ridge (H_R) is the dominant site with strongest adsorption energy. The adsorption energy is lower for the tilted on-top site on the micro facet (H_F), and is further lower for the HCP hollow site ($H_{F'}$) and the long bridge site in the trough (H_T). The result is in consistent with the LEED experimental and DFT theoretical results found in the literature. Despite the agreement, for the g-value that is a measure of the effective H-H interaction on H/Pt(110)-(1×2), the agreement with the CV experiment is not good. The g-value at lower coverage $\Theta_H < 1/3$ conditions is in reasonable agreement, and that $\Theta_H > 1/2$ is in fair agreement, while the theory predict a distinct peak at $\Theta_H \simeq 1/3$ although no such peak appears experimentally. The reason for the disagreement is not clear. Further investigation is required to explain the experimental g-value to better understand the H-adsorption on Pt(110)-(1×2).

Chapter 6

Conclusion

The numerous experimental results and their theoretical treatment reviewed in the introduction part reveal that H electroadsorption, albeit being one of the most studied electrochemical processes, are still far from being perfectly understood at the atomic level. The recent CV experimental and theoretical data give more insight into the interactions between adsorbed H atoms and the Pt surface in $HClO_4$ and H_2SO_4. However, until now, no models have been proposed to elucidate the overall properties of these isotherms.

The issues of hydrogen electroadsorption on the Pt(hkl) surface are studied to settle its theoretical description using a converged first-principles DFT-GGA calculation and a Monte Carlo simulation. The zero point energy (ZPE) correction of quantum effect, which had never been calculated in foregoing theoretical studies, had been calculated and applied to the DFT results. Therefore, by comparing these data with theory, the accuracy of theory is diagnosed. Furthermore, the effective H-H interaction, or the g-value was firstly theoretically calculated and compared with the experiment. This comparison provides important insight into the H-adsorption, which prompts further theoretical investigation.

In chapter 4, the hydrogen adsorption on the Pt(111) surface was investigated within the conventional ultrahigh vacuum (UHV) surface modeling and the semilocal Kohn-Sham level of the density functional theory (DFT). By performing a converged DFT calculation, we have confirmed nearly degenerated nature of H on the fcc hollow site (H_{fcc}) and H on the top site (H_{top}) when the nuclei are treated classically, while H_{fcc} is significantly more stable when the zero-point energy correction is applied. Relative abundance of the H_{fcc} over H_{top} was investigated by performing a Monte Carlo simulation using a lattice gas model parameterized by the DFT calculation. By comparing the calculated results with recent cyclic voltammetry data, we found good agreement between theory and experiment but minor discrepancy exists in that the H-H interaction is underestimated by $\sim$10 %.

In chapter 5, the hydrogen adsorption isotherms, evaluated by combination of density functional theory (DFT) and Monte Carlo (MC) simulations, are reported on the missing row Pt(110)-(1$\times$2) within the conventional ultrahigh vacuum (UHV) surface modeling. The binding energy for adsorption is found to depend strongly on the hydrogen coverage. The short bridge sites on the ridge (H_R) are found to be the strongest binding sites at low coverage. At higher H coverage, up to 1ML,

the on-top sites on the micro-facet (H_F) get populated. These results are shown to agree well with the LEED experimental and DFT theoretical results found in the literature. Despite the agreement, for the g-value that is a measure of the effective H-H interaction on H/Pt(110)-(1×2), the agreement with the CV experiment is not good. The reason for the disagreement is not clear. Further investigation is required to explain the experimental g-value to better understand the H-adsorption on Pt(110).

Acknowledgments

First and foremost, I would like to express the deepest appreciation to my supervisor, Professor Osamu Sugino, for his patient guidance, valued advices and kindness. His expertise in condensed matter physics improved my research skills and prepared me for future challenges.

I wish to express my sincere thanks to Dr. Yoshinari Takimoto for his helpful discussions, suggestions and generous cooperation.

I take this opportunity to record my sense of gratitude to all Sugino group's members and secretaries of the theoretical group of ISSP for their great support and encouragements.

Furthermore, I also thank Hitachi Scholarship Foundation staffs for their financial support and warm care.

Last but not the least, I am thankful and indebted to my family for their support and always encourage me to be the best.

Bibliography

[1] G.S. Karlberg, T.F. Jaramillo, E. Skúlason, J. Rossmeisl, T. Bligaard, and J.K. Nørskov, Phys. Rev. Lett. 99 (2007) 126101.

[2] K.Itaya, Prog. Surf. Sci., 58 (1998), 121.

[3] R.J. Nichols, A. Bewick, J. Electroanal. Chem. 243 (1988) 445.

[4] A. Peremans, A. Tadjeddine, Phys. Rev. Lett. 73 (1994) 3010.

[5] N. Nanbu, F. Kitamura, T. Ohsaka, K. Tokuda, J. Electroanal. Chem. 485 (2000) 128.

[6] B. Ren, X. Xu, X.Q. Li, W.B. Cai, Z.Q. Tian, Surf. Sci., 427 (1999) 157.

[7] N. M. Marković, B. N. Grgur, and P. N. Ross, J. Phys. Chem. B 101 (1997) 5405.

[8] G. Jerkiewicz, Prog. Surf. Sci. 57 (1998) 137.

[9] A. Zolfaghari, G. Jerkiewicz, J. Electroanal. Chem. 467 (1999) 177.

[10] N. M. Marković, T. J. Schmidt, B. N. Grgur, H. A. Gasteiger, R. J. Behm, P. N. Ross, J. Phys. Chem. B 103 (1999) 8568.

[11] N. M. Marković and P. N. Ross, Surf. Sci. Rep. 45 (2002) 117.

[12] M.T.M. Koper, J.J. Lukkien, N.P. Lebedeva, J.M. Feliu, R.A.V. Santen, Surf. Sci. 478 (2001) L339.

[13] M.T.M. Koper, J. Electroanal. Chem. 547 (2005) 375.

[14] A. Lasia, J. Electroanal. Chem. 562 (2004) 23.

[15] R.A. Olsen, G. J. Kores, and E.J.Baerends, J. Chem. Phys. 111 (1999) 11155.

[16] K. Nobuhara, H. Nakanishi, H. Kasai and A. Okiji, *J. App. Phys.* 88 (2000) 6897.

[17] G.W. Watson, R.P.K. Wells, D.J. Willock, G. J. Hutchings, Phys. Chem. B 105 (2001) 4889.

[18] S. C. Bădescu, P. Salo, T. Ala-Nissila, S. C. Ying, Phys. Rev. Lett. 88 (2002) 136101.

[19] S. C. Bădescu, K. Jacobi, Y. Wang, K. Bedurftig, G. Ertl, P. Salo, T. Ala-Nissila and S. C. Ying, Phys. Rev. B 68 (2003) 205401.

[20] P. Legare, J. Surf. Sci. 599 (2004) 169.

[21] D. C. Ford, Y. Xu, M. Mavrikakis, J. Surf. Sci. 587 (2005) 159.

[22] J. Greeley, M. Mavrikakis, J. Phys. Chem. B 109 (2005) 3460.

[23] G. S. Karlberg, T. F. Jaramillo, E. Skúason, J. Rossmeisl, T. Bligaard, and J. K. Nøskov, Phys. Rev. Lett. 99 (2007) 126101.

[24] E. Skúason, G. S. Karlberg, J. Rossmeisl, T. Bligaard, J. Greeley, H. Jónsson, J. K. Nøskov, Phys. Chem. Chem. Phys. 9 (2007) 3247.
[25] I. Hamada, Y. Morikawa, J. Phys. Chem. C 112 (2008) 10889.
[26] J.R. Engstrom, W. Tsai, and W.H. Wweinberg, J. Chem. Phys. 87 (1987) 3104.
[27] M. Minca, S. Penner, E. Dona, A. Menzel, E. Bertel, V. Brouet and J. Redinger, New J. Phys. 9 (2007) 386.
[28] M. Minca, S. Penner, T. Loerting, A. Menzel, E. Bertel, R. Zucca, and J. Redinger, Topics in Catalysis 46 (2007) 161.
[29] S. Gudmundsdóttir, E. Skúlason, and H. Jónsson, Phys. Rev. Lett. 108 (2012) 156101.
[30] S. Gudmundsdóttir, E. Skúlason, K.J. Weststrate, L. Juurlink, and H. Jónsson, Phys. Chem. Chem. Phys. 15 (2013) 6323.
[31] Z. Zhang, M. Minca, C. Deisl, T. Loerting, A. Menzel, E. Bertel, Phys. Rev. B 70 (2004) 121401.
[32] B.E. Conway, Ionic Hydration in Chemistry and Biophysics, Elsevier, New York (1981).
[33] B.E. Conway, G. Jerkiewicz, J. Electroanal. Chem. 357 (1993) 47.
[34] B.E. Conway, G. Jerkiewicz, Zeit. Phys. Chem. Bd. 183 (1994) 281.
[35] G. Jerkiewicz, A. Zolfaghari, J. Electrochem. Sot. 143 (1996) 1240 .
[36] M.W. Breiter, B. Kennel, Z. Elektrochem. 64 (1960) 1180.
[37] F.G. Will, C.A. Knorr, Z. Electrochem. 64 (1960) 258; 64 (1960) 270.
[38] N. Frumkin, in Advances of Electrochemistry and Electrochemical Engineering, P. Delahey (Ed.), Vol. 3, Interscience Publishers, New York (1963).
[39] K. Christmann, Surf. Sci. Rep. 9 (1988) 1.
[40] B.E. Conway, Theory and Principles of Electrode Processes,Ronald Press,London (1965).
[41] A.N. Frumkin, Electrode Processes, Nauka, Moscow (1987), in Russian.
[42] E. Gileadi, Electrode Kinetics, VCH, New York (1993).
[43] B.E. Conway, H. Angerstein-Kozlowska, H.P. Dhar, Electrochim. Acta 19 (1974) 455.
[44] J.M. Parry, R. Parsons, J. Electrochem. Soc. 113 (1966) 992.
[45] H.P. Dahr, B.E. Conway, K.M. Joshi, Electrochim. Acta 18 (1973) 789.
[46] A.N. Frumkin, B.B. Damaskin, in Modern Aspects of Electrochemistry, Vol. 3, J. O'M. Bockris, B.E. Conway, (Eds.), Butterworths, London (1964).
[47] A.N. Frumkin, O.A. Petrii, B.B. Damaskin, in Comprehensive Treatise of Electrochemistry, Vol. 1, J. O'M. Bockris, B.E. Conway, E. Yeager, (Eds.), Plenum Press,New York (1980).
[48] A. Zolfaghari, G. Jerkiewicz in Electrochemical Surface Science of Hydrogen Adsorption and Absorption, G. Jerkiewicz, P. Marcus, (Eds.), The Electrochemical Society, PV 97-16, Pennington (1997).
[49] M.J. Llorca, J.M. Feliu, A. Aldaz, J. Clavilier, J. Electroanal. Chem. 351 (1993) 299.
[50] J.M. Feliu, A. Rodes, J.M. Orts, J. Clavilier, Polish J. Chem. 68 (1994) 1575.

[51] J. Clavilier, J.M. Orts, R. Gomez, J.M. Feliu, A. Aldaz, The Electrochemical Society Proceedings vol. 94-21 (1994) 167.
[52] A. Zolfaghari, G. Jerkiewicz, J. Electroanal. Chem. 420 (1997) 11.
[53] A. Zolfaghari, G. Jerkiewicz, J. Electroanal. Chem. 422 (1997) 1.
[54] P. Ordejón, E. Artacho and J. M. Soler, Phys. Rev. B 53 (1996) R10441 .
[55] J. M. Soler, E. Artacho, J. D. Gale, A. García, J. Junquera, P. Ordejón and D. Sánchez-Portal, J. Phys.: Condens. Matter 14, (2002) 2745.
[56] P. E. Blöchl, Phys. Rev. B 50 (1994) 17953.
[57] G. Kresse and D. Joubert, Phys. Rev. B 59 (1999) 1758.
[58] G. Kresse and J. Hafner, Phys. Rev. B 47 (1993) 558; *ibid.* 49 (1994) 14251.
[59] G. Kresse and J. Furthmuller, Comp. Mater. Sci. 6, 56 (1996) 15.
[60] G. Kresse and J. Furthmuller, Phys. Rev. B 54 (1996) 11169.
[61] J. P. Perdew, K. Burke, and M. Ernzerhof, Phys. Rev. Lett., 77, (1996) 3865; *ibid.* 78 (1997) 1396.
[62] H. J. Monkhorst and D. Pack, Phys. Rev. B 13 (1976) 5188.
[63] J. Ihm, A. Zunger, and M. L. Cohen, J. Phys. C 12 (1979) 4409.
[64] W. Frank et. al., J. Phys. Rev. Lett. 74 (1995) 1791.
[65] D.J. Earl, M.W. Deem, Methods in Molecular Biology, vol. 443, Molecular Modeling of Proteins Edited by Andreas Kukol, Humana Press, Totowa, NJ (2008).
[66] V.I. Manousiouthakis, M.W. Deem, J. Chem. Phys. 110 (1999) 2753.
[67] N. Metropolis, A.W. Rosenbluth, M.N. Rosenbluth, A.N. Teller, and E. Teller, J. Chem. Phys. 21 (1953) 1087.
[68] N. Metropolis, Los Alamos Science 12 (1987) 125.
[69] G. Alefeld, J. Volkl (Ed.), Hydrogen in Metals, Parts I and II, Springer-Verlag, New York (1978).
[70] K. Christmann, G. Ertl and T. Pignet, Surf. Sci. 54 (1976) 365.
[71] P. Nordlander, S. Holloway, J.K. Nørskov, Surf. Sci. 136, (1984) 59.
[72] J. Clavilier, A. Rodes, K. Elachi, and M.A. Zamakhchari, J. de Chim. Phys. et de Physico-Chemie Biol. 7-8 (1991) 1291.
[73] B.E. Conway, G. Jerkiewicz, Electrochim. Acta 45 (2000) 4075.
[74] H. Kita, J. Mol. Catal. A: Chem. 199 (2003) 161.
[75] K. Kunimatsu, T. Senzaki, G. Samjeskė, M. Tsushima, and M. Osawa, Electrochim. Acta 52 (2007) 5715.
[76] B. Hammer, J. K. Nørskov, Nature 376 (1995) 238.
[77] T. L. Tan, L. L. Wang, D. D. Johnson, and K. Bai, J. Phys. Chem. C 117 (2013) 22696.
[78] Y. Waseda, K. Hirata, and M. Ohtani, J. High Temp. High Pressures 7 (1975) 221.
[79] L. D. Roger, B. G. Harry, Chemical structure and boding, University Science Books (1989) 199.
[80] L. D. Landau and E. M. Lifshitz, Quantum Mechanics, Elsevier Butterworth-Heinemann, Oxford (1958) 319.

[81] S. Hong and T. S. Rahman, R. Heid, and K. P. Bohnen, Phys. Rev. B 71 (2005) 245409.

[82] K. Fukutani, A. Itoh, M. Wilde, and M. Matsumoto, Phys. Rev. Lett. 88 (2002) 116101.

[83] B. Hammer, L. B. Hansen, and J. K. Nørskov, Phys. Rev. B 59 , 7413 1999.

[84] G. Källén and G. Whanström, Phys. Rev. B 65 (2001) 033406.

[85] G. Henkelman and H. Jonsson, J. Phys. Rev. Lett. 86 (2000) 664.

[86] M. Baldauf and D. M. Kolb, J. Electrochim. Acta 38 (1993) 2145.

[87] M. Matsumoto and T. Nishimura, ACM Trans. Model. Comput. Simul. 8 (1998) 3.

[88] T.T.T. Hanh, Y. Takimoto, O. Sugino, Surf. Sci. 625 (2014) 104.

[89] C.R. Henry, Surf. Sci. Rep. 31 (1998) 231.

[90] S. Dahl, A. Logadóttir, R.C. Egeberg, J.H. Larsen, I. Chorkendorff, E. Törnqvist and J.K. Nørskov, Phys. Rev. Lett. 83 (1999) 1814.

[91] B. Hvolbaek, T.V.W. Janssens, B. C. Clausen, H. Falsig, C.H. Christensen and J.K. Nørskov, Nano Today 2 (2007)14.

[92] S. Gudmundsdóttir, W. Tang, G. Henkelman, H. Jónsson and E. Skúlason, J. Chem. Phys. 137 (2012) 164705.

[93] E. Skúlason, G.S. Karlberg, J. Rossmeisl, T. Bligaard, J. Greeley, H. Jónsson and J.K. Nørskov, Phys. Chem. Chem. Phys., 9 (2007) 3241.

[94] G. Anger, H.F. Berger, M. Luger, S. Feistritzer, A. Winkler and K.D. Rendulic, Surf. Sci. 219 (1989) L583.

[95] C.S. Shern, Surf. Sci. 264 (1992) 171.

[96] G. Burns, Solid State Physics (Academic, New York, 1985).

[97] W. Stenzel, S. Jahnke, Y. Song, and H. Conrad, Prog. Surf. Sci. 35 (1991) 159.

[98] E. Kirsten, G. Parschau, W. Stocker, and K. Rieder, Surf. Sci. 231 (1990) L183.

[99] C. Lu and R.I. Masel, J. Phys. Chem. B 105 (2001) 9793.

[100] V. Blum, L. Hammer, K. Heinz, C. Franchini, J. Redinger, K. Swamy, C. Deisl, and E. Bertel, Phys. Rev. B 65 (2002) 165408.